On the atmospheric budget of 1,2-dichloroethane ~~ethylene dichloride~~ and its impact on stratospheric chlorine and ozone (2002-2020)

Ryan Hossaini[1], David Sherry[2], Zihao Wang[3,4], Martyn P. Chipperfield[3,5], Wuhu Feng[3,6], David E. Oram[7,8], Karina E. Adcock[8], Stephen A. Montzka[9], Isobel J. Simpson[10], Andrea Mazzeo[1], Amber A. Leeson[1], Elliot Atlas[11], and Charles C.-K Chou[12].

[1]Lancaster Environment Centre, Lancaster University, Lancaster, UK.
[2]Nolan Sherry and Associates (NSA), London, UK.
[3]School of Earth and Environment, University of Leeds, Leeds, UK.
[4]Department of Ocean Sciences and Engineering, Southern University of Science and Technology, Shenzhen, China.
[5]National Centre for Earth Observation, University of Leeds, Leeds, UK.
[6]National Centre for Atmospheric Science, University of Leeds, Leeds, UK.
[7]National Centre for Atmospheric Science, University of East Anglia, Norwich, UK.
[8]School of Environmental Sciences, University of East Anglia, Norwich, UK.
[9]NOAA Global Monitoring Laboratory (GML), Boulder, CO, USA.
[10]Department of Chemistry, University of California-Irvine, Irvine, CA, USA.
[11]Department of Atmospheric Sciences, RSMAS, University of Miami, Miami, Florida, USA.
[12]Research Center for Environmental Changes, Academia Sinica, Taipei, Taiwan.

Correspondence to: Ryan Hossaini (r.hossaini@lancaster.ac.uk)

Abstract. 1,2-dichloroethane (DCE), or ~~E~~ethylene dichloride ~~(EDC), or 1 2 dichloroethane,~~, is an industrial very short-lived substance (VSLS) whose major use is as a feedstock in the production chain of polyvinyl chloride (PVC). Like other chlorinated VSLS, transport of ~~EDC~~ DCE (and/or its atmospheric oxidation products) to the stratosphere could contribute to ozone depletion there. However, despite annual production volumes greatly exceeding those of more prominent VSLS (e.g. dichloromethane), global DCE~~EDC~~ observations are sparse, thus the magnitude and distribution of DCE~~EDC~~ emissions and trends in its atmospheric abundance are poorly known. In this study we performed an exploratory analysis of the global DCE~~EDC~~ budget between 2002 and 2020. Combining bottom-up data on annual production and assumptions around fugitive losses during production and feedstock use, we assessed the DCE~~EDC~~ source strength required to reproduce atmospheric DCE~~EDC~~ observations. We show that the TOMCAT/SLIMCAT 3-D chemical transport model (CTM) reproduces DCE~~EDC~~ measurements from various aircraft missions well, including HIPPO (2009-2011), ATom (2016-2018) and KORUS-AQ (2016), along with surface measurements from South East Asia, when assuming a regionally varying production emission factor in the range 0.5-1.5%. Our findings imply substantial fugitive losses of DCE~~EDC~~ and/or substantial emissive applications (e.g. solvent use) that are poorly reported. We estimate DCE~~EDC~~'s global source increased by ~45% between 2002 (349±61 Gg/yr) and 2020 (505±90 Gg/yr) with its contribution to stratospheric chlorine increasing from 8.2 (±1.5) ppt Cl to ~12.9 (±2.4) ppt Cl over this period. DCE~~EDC~~'s relatively short overall tropospheric lifetime (~83 days) limits, though does not preclude, its transport to the stratosphere and we show that its impact on ozone is small at present. Annually averaged, DCE~~EDC~~ is estimated to have decreased ozone in the lower stratosphere by up to several ppb (<1%) in 2020,

though a larger effect in the springtime Southern Hemisphere polar lower stratosphere is apparent (decreases of up to ~1.3%). Given strong potential for growth in ~~EDC~~ DCE production tied to demand for PVC, ongoing measurements would be of benefit to monitor potential future increases in its atmospheric abundance and its contribution to ozone depletion.

1 Introduction

40 Very short-lived substances (VSLS) are a class of halogenated chemicals with local surface lifetimes typically less than ~6 months, leading to spatial and temporal heterogeneity in their tropospheric abundance (e.g. WMO, 2018, 2022). Despite short lifetimes relative to long-lived ozone-depleting substances (ODSs) controlled by the Montreal Protocol, such as chlorofluorocarbons (CFCs) and hydrofluorocarbons (HCFCs), a range of both natural and anthropogenic VSLS have been detected in the lower stratosphere (e.g. Laube et al., 2008; Hossaini et al., 2019; Keber et al., 2020). This has motivated

45 research into the possible impacts of VSLS on stratospheric ozone and ozone trends (e.g. Salawitch et al., 2005; Feng et al., 2007; Falk et al. 2017; Bednarz et al., 2022, 2023; Villamayor et al., 2023). The most prominent VSLS with significant industrial sources are chlorinated compounds (Cl-VSLS), including dichloromethane (CH_2Cl_2) and chloroform ($CHCl_3$). These gases have a non-zero ozone depletion potential (ODP, Claxton et al., 2019) and global emissions of both have increased considerably in recent years, particularly from Asia (e.g. Hossaini et al., 2017; Fang et al., 2019; Say et al., 2019;

50 Claxton et al., 2020; An et al., 2021, 2023).

The molecule 1,2-dichloroethane (CH_2ClCH_2Cl, DCE), also known commonly as ethylene dichloride (EDC), is a further chlorinated VSLS, produced industrially in large volumes worldwide. In the USA, for instance, some ~9,000-14,000 Gg of DCE~~EDC~~ are estimated to have been produced annually in the period 2011 to 2015 (ATSDR, 2022) and global total

55 production capacity in 2020 was estimated at ~60,000 Gg (TEAP, 2022). DCE~~EDC~~'s main use is as a chemical intermediate in the manufacture of vinyl chloride monomer (VCM), a raw material in the production of the widely used plastic, polyvinyl chloride (PVC). Over 95% of DCE~~EDC~~ consumption is estimated to be in VCM production (UNEP, 2002; ECHA, 2012; CEH, 2023) which, in principle, is a largely non-emissive application (i.e. because DCE~~EDC~~ is consumed in reaction). Like other halocarbons however, fugitive release of ~~EDC~~ DCE to the atmosphere may occur during its production, storage and

60 transportation (TEAP, 2022). Other known but relatively minor uses of DCE~~EDC~~ include: (1) in the production of other chemicals, such as ethyleneamines (e.g. Ayres and Ayres, 1997), (2) historically, as a lead scavenger in fuels (e.g. Falta et al., 2005), and (3) in various applications on account of being an effective solvent, such as metal degreasing (EPA, 2020), and in organic and medicinal chemistry (e.g. Jordon et al., 2021). Due to concern over its toxicity, regulatory controls restricting commercial DCE~~EDC~~ uses are in place in some regions, including the European Union (Sherwood et al., 2018)

65 where DCE~~EDC~~ was placed in Annex XIV of the EU's REACH (Registration, Evaluation, Authorisation and Restriction of Chemicals) regulation in 2016.

In contrast to other major chlorinated VSLS (e.g. CH$_2$Cl$_2$, CHCl$_3$, C$_2$Cl$_4$), the National Oceanic and Atmospheric Administration (NOAA) and Advanced Global Atmospheric Gases Experiment (AGAGE) global monitoring networks do not yet routinely report surface ~~EDC~~ DCE measurements and there are no other archived long-term observational records. In consequence, the global ~~EDC~~ DCE budget and trends in its atmospheric abundance are poorly known. The current paucity of global ~~EDC~~ DCE surface measurements also prevents the assessment of its global source using top-down inverse methods, as performed for other industrial VSLS (Claxton et al., 2020). Measurements of ~~EDC~~ DCE from a limited number of aircraft campaigns in various world regions indicate typical Northern Hemisphere (NH) boundary layer mole fractions in the range ~10-20 ppt (Engel and Rigby et al., 2018; Roozitalab et al., 2024). However, far larger levels have also been detected in East and South-East Asia, including mole fractions >1 ppb in China at ~~reportedly~~ both urban and background sites (Lyu et al. 2020 & references therein). Based on air samples obtained from surface sites in Taiwan and Malaysia in 2013 and 2014, Oram et al (2017) reported median ~~EDC~~ DCE mole fractions of 85.4 (16.7–309) ppt and 21.7 (16.4–120) ppt, respectively, with a strong correlation of ~~EDC~~ DCE with CH$_2$Cl$_2$ observed at both sites. Combining this relationship with a bottom-up estimate of regional CH$_2$Cl$_2$ emissions, the same study inferred Chinese ~~EDC~~ DCE emissions to be of the order of 203 (±9) Gg/yr for the period 2013/14.

Based on a combination of high-altitude aircraft observations and modelling, Cl-VSLS were estimated to provide ~130 (100-160) ppt Cl to the stratosphere in 2019 (Laube and Tegtmeier et al., 2022). Although this represents just ~4% of total stratospheric chlorine (which principally is from long-lived ODSs that are now controlled by the Montreal Protocol), increasing VSLS amounts have slowed the rate at which chlorine is decreasing in the stratosphere (Hossaini et al., 2019; Bednarz et al., 2022). Additionally, far larger local injections of Cl-VSLS (including ~~EDC~~DCE) into the Northern Hemisphere (NH) extratropical lower stratosphere (LS) have been reported (Adcock et al., 2021; Lauther et al., 2022), reflecting transport via the Asian summer monsoon anticyclone and the co-location of relatively strong Asian emissions with efficient vertical ascent (e.g. Randel et al., 2010). While CH$_2$Cl$_2$ remains the largest contributor to stratospheric chlorine from VSLS (Laube and Tegtmeier et al., 2022), the large volumes of ~~EDC~~ DCE produced worldwide, its substantial global trade, and the potential for future growth tied to PVC demand (e.g. in the building and construction industries) means it is of interest to establish DCE~~EDC~~'s present-day atmospheric budget and fate.

In this study, we have analysed global ~~EDC~~ DCE production data between 2002 and 2020 and used it to create a set of gridded global emissions for different assumed emission factors describing fugitive ~~EDC~~ DCE losses. Using the TOMCAT/SLIMCAT 3-D chemical transport model (CTM), we evaluated the realism of these emissions by assessing the model's ability to reproduce various aircraft measurements of ~~EDC~~DCE, thereby providing new constraints on its global source. The CTM was used to quantify the likely contribution of ~~EDC~~ DCE and its products to stratospheric chlorine and thus the potential impact of ~~EDC~~ DCE emissions on stratospheric ozone. The paper is structured as follows. Section 2 describes our approach to creating the ~~EDC~~ DCE emission inventories, as well as the CTM, the simulations performed, and

observational datasets used. Our results are presented in Section 3, including on the inferred magnitude of global DCE~~EDC~~ emissions (Section 3.1), DCE~~EDC~~'s budget and contribution to stratospheric chlorine (Section 3.2), and DCE~~EDC~~'s impact on stratospheric ozone (Section 3.3). A summary of key findings and concluding remarks is given in Section 4.

2. Data, Methods and Model

2.1 Bottom-up data on EDC production

DCE~~EDC~~ is manufactured industrially via the direct chlorination of ethene or via its oxychlorination with hydrogen chloride. Estimated annual ~~EDC~~ DCE production data were compiled biennially by Nolan Sherry Associates (NSA) over the period 2002 to 2020 (**Table 1**). Data from NSA were reported in the most recent Technology and Economic Assessment Panel (TEAP) report to the parties of the Montreal Protocol (TEAP, 2022) and have been utilised in a range of recent scientific papers (e.g. Chipperfield et al., 2018; Claxton et al., 2020). Analysis by NSA makes use of their extensive database of halocarbon production and production capacities, industry data, and public reports, and is refined through industry dialogue. NSA's analysis of DCE~~EDC~~ production includes assessment of downstream products (VCM and PVC), accounting for several specific industry and market factors and trade movements. This includes the fact that VCM production may not always occur via the "ethylene route", which uses DCE~~EDC~~ at a rolling ratio of 1.6 units ~~EDC~~ DCE to VCM, but the "acetylene route", which involves the direct production of VCM from acetylene's reaction with hydrogen chloride (i.e. no DCE~~EDC~~ involved). The latter approach is prevalent in, for example, China, meaning that Chinese DCE~~EDC~~ production is relatively modest compared to other major global economies. Note that at the country level, some of the data available to NSA are proprietary in nature and confidential. On this basis and to aid the discussion and presentation, data have been aggregated into 13 broader geographical regions for which we discuss production and emissions. These regions cover all the world's major industrialised zones and their boundaries (**Figure 1**) are based on the region definitions used in Phase 2 of the Hemispheric Transport of Air Pollution (HTAP) project (e.g. Huang et al., 2017).
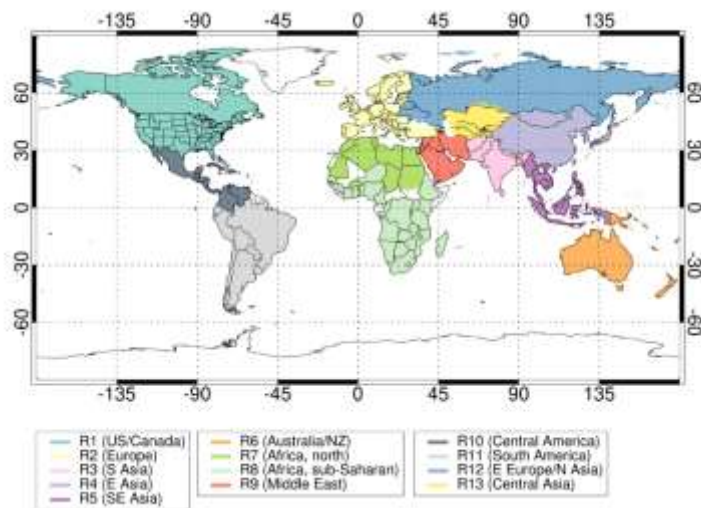
Figure 1. *Definitions of the 13 geographical regions considered for ~~EDC~~ DCE production and emissions*

Evident from the data in **Table 1** is that ~~EDC~~ DCE is produced in large quantities (~52,000 Gg in 2020) and that global production increased by ~29% between 2002 and 2020. North America, Europe, and S, E and SE Asia (regions 1-5) are estimated to account for ~86% of world production in 2020. Noting that the end-product of DCE~~EDC~~'s principal industrial use (i.e. PVC) is closely followed and reported on by both business performance analysts and environmentalists, the production data from NSA is estimated to be accurate to within around ±5%. Although estimates of DCE~~EDC~~ production in peer-reviewed literature are scarce, some independent figures exist with which to compare. For instance, data cited by the U.S. Environmental Protection Agency (EPA) places the annual volume of DCE~~EDC~~ produced in the USA at 12,750 Gg in 2011 (EPA, 2020). Interpolating between years on either side (recalling that production data from NSA was provided biennially), the corresponding U.S. production from NSA is 13,145 Gg (2011), i.e. in close agreement with U.S. EPA figure (within ~3%). An assessment around health aspects of DCE~~EDC~~ exposure placed European production at more than 10,000 Gg per annum (Cherrie et al., 2011), consistent with the NSA data in **Table 1**. Few estimates of DCE~~EDC~~ production in Asia exist in the peer-reviewed literature. However, an estimate of Chinese DCE~~EDC~~ production in the year 2010 of 2,708 Gg (Chinabaogao, 2012) is very similar to that for China from NSA in the same year (2,700 Gg).

Table 1. *Estimated annual production of ~~EDC~~ DCE (Gg) from NSA in the 13 world regions in Figure 1.*

R#	Region name	2002	2004	2006	2008	2010	2012	2014	2016	2018	2020
1	US/Can	14429	14929	13894	12649	12789	13499	14199	16199	18199	16749
2	Europe	11176	11757	12055	11300	11680	11771	11739	11799	11749	11499

3	S Asia	284	257	239	274	449	479	399	423	457	444
4	E Asia	8951	9545	10563	10642	10771	10534	10723	11738	13889	14147
5	SE Asia	1114	1249	1239	1409	1549	1759	1799	2014	2153	2199
6	Aus/NZ	0	0	0	0	0	0	0	0	0	0
7	Afr. N	117	144	144	139	137	224	314	314	339	555
8	Afr. Sub-S	207	175	207	151	263	223	263	271	263	239
9	Mid. East	1636	1830	2076	1817	2552	2807	2924	3339	3436	3327
10	Cen. Am.	394	279	524	579	639	629	609	89	89	89
11	S Am.	1129	1234	1379	1639	1559	1429	1579	1609	1389	999
12	E Eur/N Asia	1011	976	1294	1274	1214	1034	1179	1359	1819	1889
13	Cen. Asia.	0	0	0	0	0	0	0	0	0	0
	Global total	**40457**	**42384**	**43623**	**41882**	**43611**	**44398**	**45737**	**49164**	**53792**	**52146**

Table 2. *As Table 1 but for consumption.*

R#	Region name	2002	2004	2006	2008	2010	2012	2014	2016	2018	2020
1	US/Can	13024	13503	12827	11826	12103	12744	12955	14867	16882	15252
2	Europe	10980	11632	11975	11114	11354	11463	11539	11503	11646	11327
3	S Asia	579	526	540	569	798	1016	993	1066	1307	1186
4	E Asia	10718	11510	11920	11712	11836	11373	11960	12935	14642	14595
5	SE Asia	1365	1423	1498	1742	1848	1967	1834	2339	2492	2545
6	Aus/NZ	<1	<1	<1	<1	<1	<1	<1	<1	<1	<1
7	Afr. N	118	145	145	140	147	260	448	482	536	1011
8	Afr. Sub-S	202	175	208	152	264	224	264	281	264	240
9	Mid. East	1095	1234	1458	1264	1990	2265	2386	2627	2614	2603
10	Cen. Am.	390	284	535	568	662	631	610	91	106	90
11	S Am.	1036	1008	1223	1580	1395	1415	1563	1610	1479	1403
12	E Eur/N Asia	944	938	1288	1246	1210	1034	1179	1360	1820	1890
13	Cen. Asia.	<1	<1	<1	<1	<1	<1	<1	<1	<1	<1
	Global total	**40457**	**42384**	**43623**	**41882**	**43611**	**44398**	**45737**	**49164**	**53792**	**52146**

145   The demand for ~~EDC~~ DCE in both producing and non-producing countries was evaluated from trade data. Net imports (gross imports minus gross exports) were calculated for a total of ~150 countries over our study period (2002-2020) using publicly available trade statistics accessed via the online UN Comtrade Database (https://comtradeplus.un.org/). Assuming global imports should equal global exports in a given year, net imports should sum to zero across the globe. However, due to imperfections in reported trade data (known to afflict many commodities besides DCE~~EDC~~) this was found not to be the

150   case. Although the imbalance was small (average of ~7% over our study period expressed as the difference between gross imports and exports) compared to the large production volumes of DCE~~EDC~~, we elected to reconcile the trade data using the method of Zou et al. (2023). Briefly, where a record of DCE~~EDC~~ trade is recorded by the importer but not the exporter (or vice versa), the missing trade is filled in. Where records match but the trade quantities differ, the larger of the two was adopted (Zou et al., 2023). This approach balances global DCE~~EDC~~ trade and prevents errors in trade statistics from

155   confounding our subsequent analysis.

2.2 ~~EDC~~ DCE emissions

Emissions of ~~EDC~~ DCE may in principle arise during its (1) production, (2) use as a feedstock, (3) transportation, and (4) any emissive uses (e.g. as a solvent). Items 1-3 represent fugitive emissions that may arise from, for example, the operation and maintenance of chemical plants, along with bulk storage and other industrial processes where unintended leakage can

160   occur. In a fully explicit bottom-up inventory, production emissions may be calculated as the product of annual ~~EDC~~ DCE production and a suitable emission factor. Similarly, feedstock use emissions, which are additional and additive, may be calculated from the quantity of ~~EDC~~ DCE used as feedstock and a further emission factor (e.g. TEAP, 2022). However, although ~~EDC~~ DCE is principally used as a feedstock in the manufacture of VCM, with some assessments placing this use at >98% (CEH, 2023), the precise quantity and how this may have varied over time and across regions is unknown. Note, even

165   if 98% of ~~EDC~~ DCE use is in producing VCM, this does not imply that the remaining 2% is used in emissive applications. This is because ~~EDC~~ DCE also finds use as an intermediate in the production of other chemicals, including ethyleneamines and other chlorinated solvents (Section 1; TEAP, 2022). Analysis by NSA suggests that these two sectors contribute of the order 600-800 Gg/yr of ~~EDC~~ DCE feedstock use. In our idealised framework for calculating ~~EDC~~ DCE emissions we assume that 100% of ~~EDC~~ DCE use (consumption) is as feedstock.

170

The annual total ~~EDC~~ DCE emission per country in year t was calculated using **Equation 1**.

$$Emission(t) = P(t)\alpha_1 + C(t)\alpha_2 + I(t)\alpha_3 \qquad (1)$$

The first term on the right denotes production emissions calculated from the time-varying production (P) data provided by

175   NSA. There are 36 producing countries in the NSA database to which this term applies. The second term on the right denotes feedstock use emissions calculated based on consumption (C) data. Consumption (production + net imports) was calculated

for ~150 countries in total. The DCEEDC-producing countries dominate global consumption, with non-producers accounting for less than 0.6% of the global total. Production and consumption data in **Tables 1** and **2** are aggregated regional totals obtained from country-level analysis. The third term on the right of Equation 1 represents fugitive emissions during supply

180   chain. We have elected to apply these in the country of import and they are calculated from gross import (I) data.

In Equation 1, emission factors for production, feedstock use, and supply chain emissions are denoted by α_1, α_2, and α_3, respectively. Tight emission controls throughout the whole EDC DCE production cycle and its supply chain, especially in more developed countries, are expected to occur to minimise loss of useful material, to control costs in an extremely competitive industry, and also for possible legal compliance. For EDCDCE, all α values in developed countries are thus

185   expected to be small and likely to lie towards the lower end of the plausible ranges reported in the literature for other gases (TEAP, 2022). For context, fugitive emissions from production of other halocarbons have typically been estimated at ~0.5% on production (IPCC/TEAP, 2005). However, due to differences in plant operations and regulatory requirements in different world regions, regional differences in emission factors are likely. For EDCDCE, we examined a range of emission factors around the above value, varying α_1 between 0.1% through to 0.6% for developed countries. For developing countries,

190   approximated as those operating under Article 5 (A5) of the Montreal Protocol, we assume a multiplier of 3. The different scenarios are labelled according to their developed country α_1 emission factor (see **Table 3**). Fugitive emissions from feedstock uses are generally expected to be lower than those from production (TEAP, 2022). We assumed a fixed feedstock emission factor of $\alpha_2 = 0.1\%$, representing the "low" estimate reported by TEAP (2022). Note, where consumption is negative (i.e. exports exceed production plus imports), we assume no feedstock use emission. Similarly, we adopt a fixed

195   supply chain emissions factor of $\alpha_3 = 0.1\%$, representing the "low" estimate for distribution emissions reported by TEAP (2022). The resulting estimated range of total fugitive emissions is 146-594 Gg/yr in 2020 (**Table 3**).

Many modern DCEEDC-producing plants are integrated on-site with VCM/PVC production (Cherrie et al., 2011). If the processes are seamless, the distinction between fugitive losses from production and fugitive losses from feedstock use may be less clear cut compared with other gases. An alternative framework (not adopted) thus might be to consider a single

200   emission factor, applied to production, that encapsulates all possible leakage over DCEEDC's internal lifetime within a plant. As we elected to consider global trade, and hence use consumption in conjunction with production, it was necessary to treat the two terms separately. We note that our overarching goal is to examine the impact of EDC DCE on stratospheric ozone using a global model calibrated to reproduce tropospheric observations of DCEEDC. The overall magnitude and location of EDC DCE emissions is thus important, but the detail of the fugitive source is secondary.

205   For inclusion in the CTM, the calculated biennial EDC DCE emissions (**Table 3**) were linearly interpolated to give annual records over the 19-year study period (2002 to 2020). The emissions were aggregated onto a global 0.5°×0.5° grid using the country mask of Perrette (2023). This mask was developed for the Inter-Sectoral Impact Model Intercomparison Project (ISIMIP). The within-country EDC DCE distribution was assumed to follow that of ethene. The reaction of ethene with chlorine is the main route by which industrial EDC DCE production occurs and thus ethene should be a reasonable proxy.

210   Anthropogenic ethene emissions (year 2014) from the 'industrial combustion and processes' sector were taken from the gridded (0.5°×0.5°) datasets produced for CMIP6 (Feng et al., 2020). **Figure 2** illustrates the resulting surface DCE~~EDC~~ emission distribution and timeseries of regional and global emissions for 'scenario sc05', i.e. with $\alpha_1 = 0.5\%$ (non-A5) / 1.5% (A5). In this example case, Asia (sum of Regions 3-5) accounts for ~48% of global emissions in 2020. For other Cl-VSLS, Asian emissions have been assessed to dominate the global anthropogenic source, such as the estimated ~90%

215   contribution of Asia to global CH_2Cl_2 emissions reported by Claxton et al. (2020). For DCE~~EDC~~, the approach and information described above gives rise to a more even distribution of emissions between continents, including a sizeable source outside of Asia.

Table 3. *Estimated global ~~EDC~~ DCE emissions (Gg) due to fugitive losses between 2002 and 2020 (assuming 100% of ~~EDC~~ DCE consumption is for feedstock use) and for different assumed production emission factors (α_1)*

220   *in non-Article 5 (developed) and Article 5 (developing) countries.*

Scenario	α_1 (%)		Global ~~EDC~~ DCE emission (Gg / yr)									
	non-A5	A5	2002	2004	2006	2008	2010	2012	2014	2016	2018	2020
sc01	0.1	0.3	105	111	116	114	120	123	127	136	150	146
sc02	0.2	0.6	166	175	185	183	193	199	204	218	241	236
sc03	0.3	0.9	227	239	254	251	266	274	282	301	333	325
sc04	0.4	1.2	288	304	323	320	339	349	359	384	425	415
sc05	0.5	1.5	349	368	392	389	412	425	437	467	516	505
sc06	0.6	1.8	410	433	461	458	485	500	515	549	608	594
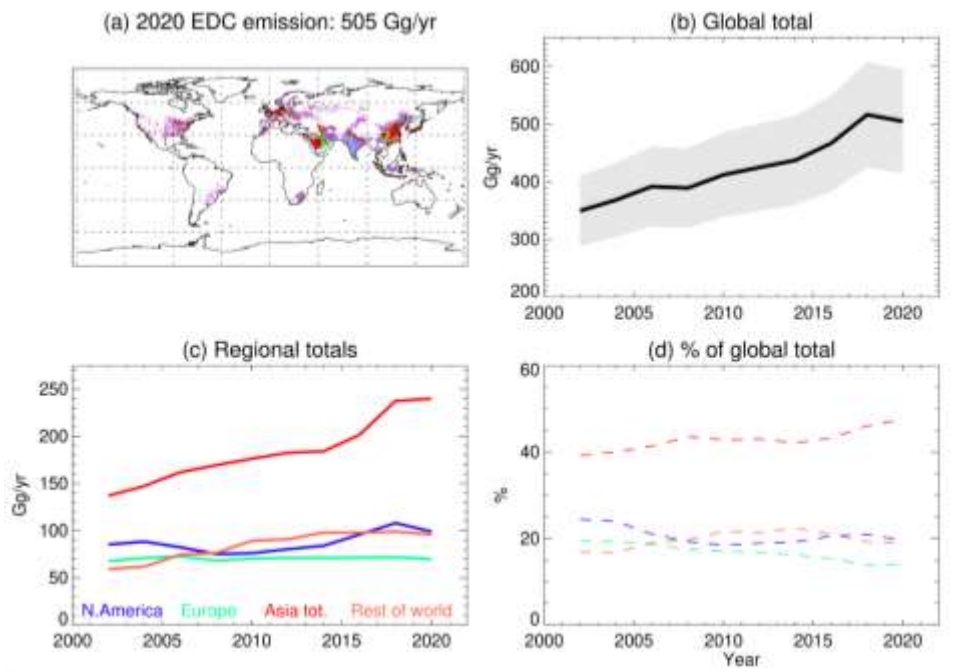
Figure 2. (a) Estimated global surface ~~EDC~~ DCE emission distribution in Jan 2020 (10^{-2} kg/m²/s). (b) Global total ~~EDC~~ DCE emission vs year (Gg/yr). (c) Regional total ~~EDC~~ DCE emissions vs year. (d) Proportion of global ~~EDC~~ DCE emissions by region (%). All data based on scenario sc05 (i.e. assuming $\alpha_1 = 0.5$ or 1.5%) with the lower/upper uncertainty (grey shading) in panel b denoting the sc04 and sc06 cases.

2.3 CTM and experiments

The time-varying ~~EDC~~ DCE emissions described in Section 2.2 were included in the TOMCAT/SLIMCAT 3-D CTM (Chipperfield, 2006). The model is well evaluated and has been widely used to study the atmospheric budget and impacts of a range of trace gases, including VSLS (e.g. Claxton et al., 2020; Hossaini et al., 2019). The offline model (hereafter 'TOMCAT') is forced by meteorological fields from the European Centre for Medium-Range Weather Forecasts (ECMWF) ERA5 dataset (Hersbach et al., 2020). The model uses the Prather (1986) scheme for tracer advection and the Holtslag and Boville (1993) scheme to represent boundary layer mixing. For convective transport, the model here utilised archived convective mass fluxes from ERA5. This approach was previously evaluated for ERA-Interim by Feng et al. (2011) and found to perform well. All simulations were performed at a 2.8°×2.8° (T42 Gaussian grid) horizontal resolution and with 60 hybrid sigma-pressure (σ-p) levels extending from the surface to ~60 km.

To test model-measurement agreement under different ~~EDC~~ DCE scenarios, and thus provide constraint on the global ~~EDC~~ DCE source strength, a reduced chemistry configuration of the CTM was used. In this configuration, the concentration of the

240 hydroxyl radical (OH) was prescribed from the monthly-varying climatology produced for the Tracer Transport Model Intercomparison Project (TransCom) on methane (Patra et al., 2011). Six simulations were performed in which the model DCE~~EDC~~ tracer was controlled by differing surface emissions (**Table 3**), along with transport, and oxidation by OH. The rate constant for the DCE~~EDC~~ + OH reaction (k_{OH}) was specified from the latest Jet Propulsion Laboratory (JPL) kinetics evaluation (Burkholder et al., 2019): $k_{OH} = 1.14 \times 10{-}11 \exp(-1150/T)$. The reaction was assumed to proceed as: ~~EDC~~ DCE

245 + OH → 2Cl + products. There is no current recommendation given for ~~EDC~~ DCE absorption cross sections and, like other chlorinated VSLS, photolysis is expected to be a minor tropospheric sink (Carpenter and Reimann et al., 2014) and so was not considered. Deposition was not included as a DCE sink but is expected to be relatively minor.

For diagnosing DCE~~EDC~~'s contribution to stratospheric chlorine and its effect on ozone, we used a CTM configuration with 'full' stratospheric chemistry. This configuration includes a treatment of all major processes that control polar and extra-

250 polar ozone (e.g. Chipperfield et al., 2018). Full chemistry simulations considered only the most likely range of DCE~~EDC~~ emissions (determined in Section 3.1) and the DCE~~EDC~~ tracer was treated as described above. In the troposphere, chlorine atoms released from DCE~~EDC~~ oxidation will quickly speciate into HCl, the dominant inorganic chlorine (Cl_y) reservoir (e.g. via $CH_4 + Cl \rightarrow HCl$ + products). Tropospheric removal of HCl and other Cl_y species (HCl, HOCl and $ClONO_2$) through wet and dry deposition was calculated with the standard tropospheric TOMCAT routines (Giannakopoulos et al., 1999; Monks et

255 al., 2017). Henry's law data used to calculate wet deposition rates were taken from Sander et al. (2023). Full chemistry model runs were spun-up for 10 years and then run over the full 19-year analysis period (2002-2020). The stratospheric chlorine and ozone response to DCE~~EDC~~ emissions were diagnosed from paired simulations (i.e. comparing runs with ~~EDC~~ DCE emissions to a no-DCE~~EDC~~ control run). Time-varying surface mixing ratios of long-lived gases (halogenated ODSs, N_2O, CH_4 etc) were prescribed from the data given in WMO (2018).

260 **2.4 ~~EDC~~ DCE observations**

We have utilised a range of aircraft measurements of ~~EDC~~ DCE to evaluate the model and to provide constraints on the global ~~EDC~~ DCE source strength. The HIAPER Pole-to-Pole Observation (HIPPO) mission (e.g. Wofsy et al., 2011) was conducted between 2009 and 2011 and involved measurements of a wide range of trace gases predominately over the Pacific from on board the National Science Foundation (NSF) Gulfstream V aircraft. Sampling extended over a large latitude range

265 from roughly the North Pole to the Antarctic Ocean and from the surface to ~14 km. The mission comprised 5 campaigns conducted in different seasons: HIPPO-1 (January 2009), HIPPO-2 (November 2009), HIPPO-3 (March-April 2010), HIPPO-4 (June 2011) and HIPPO-5 (August/September 2011). Measurements of ~~EDC~~ DCE were obtained by the University of Miami based on the analysis of whole air samples collected in flask samples during each campaign.

The more recent NASA Atmospheric Tomography (ATom) mission was conducted between 2016 and 2018 also involved

270 extensive measurements of trace gases from near pole to pole, including over the Pacific and the Atlantic. Measurements were obtained up to an altitude of ~12 km on board the NASA DC-8 aircraft over 4 campaigns covering different seasons:

ATom-1 (July-August 2016), ATom-2 (January-February 2017), ATom-3 (September-October 2017), and ATom-4 (April-May 2018). An overview of the ATom mission including some scientific highlights is given in Thompson et al. (2022). For this study, we have used ~~EDC~~ DCE measurements obtained by NOAA from air samples collected with the Programmable

275 Flask Package (PFP) whole air sampler. The EDC measurement precision is around 1% on average (for mole fractions of 1-2 ppt) and the detection limit is <1 ppt. Regarding sample stability, the NOAA ATom sampling was conducted via pressurization into glass flasks, and there has been no indication of systematic growth or destruction of DCE in glass flasks over time within the measurement precision. Like HIPPO, the spatial coverage of ATom makes it an especially useful dataset with which to evaluate global models (e.g. the representation of hemispheric gradients). In our subsequent analysis,

280 data from both HIPPO and ATom have been aggregated into 9 latitude bins (>80°N, 60-80°N, 40-60°N, 20-40°N, 0-20°N, 0-20°S, 20-40°S, 40-60°S and <60°S). The mean, standard deviation, and number of datapoints for each bin (boundary layer only, <3km) is given in **Table 4**.

To examine model performance over Asia, we also used measurements obtained during the 2016 Korea-United States Air Quality Study (KORUS-AQ) mission. The mission took place in the months of May and June and included 20 research

285 flights of the NASA DC-8 aircraft based from Osan Air Base, approximately 50 km south of Seoul, South Korea (Crawford et al., 2020). Measurements during this campaign targeted local urban sources of photochemical pollutants and therefore the air sampled differs considerably from that sampled during HIPPO and ATom. Measurements of ~~EDC~~ DCE and other gases were obtained from whole air samples collected by the University of California, Irvine (UCI) from the surface up to an altitude of ~11 km. The measurement detection limit was 0.1 pptv and the measurement precision was 5% (Simpson et al.,

290 2020). The UCI group has run extensive tests on the stability of compounds in their canisters in the time between sampling and analysis, and DCE is stable within the canisters. Highly elevated levels of ~~EDC~~ DCE and other VOCs were reported from KORUS-AQ, especially in airmasses originating from China (Simpson et al., 2020). For the analysis here, the ~~EDC~~ DCE mole fractions were aggregated into 8 altitude bins (0-8 km) of 1 km depth. Sampling was extensive and the number of measurements in each bin ranged from 94 to 1323.

295 To further evaluate model performance over eastern Asia, we used surface ~~EDC~~ DCE measurements made by the University of East Anglia (UEA) at Bachok Marine Research Station, which lies on the North East of Malaysia (6.009°N, 102.425°E), and at two sites in Taiwan: (1) Fuguei Cape, on the northern Taiwanese coast (25.297°N, 121.538°E), and (2) Hengchun, on the southern coast (22.0547°N, 120.6995°E). Measurements of ~~EDC~~ DCE and other Cl-VSLS at each location have been reported by Oram et al. (2017) and show elevated levels with respect to data obtained in other world regions. The same study

300 provides full details of the sampling and instrument method. Briefly, measurements were obtained by whole air samples collected between 2014 and 2020. Sampling is seasonal and targeted primarily at observing emissions from East Asia during the NE monsoon. Sampling at Bachok occurred in the months of November to March, while sampling at Fuguei Cape (2014 and 2016 onwards) and Hengchun (2013 and 2015 only) mostly occurred in March to May (**Table S1** in Supplement). The latter two sites in Taiwan are combined to give a single time-series in our subsequent analysis. UEA samples were collected

305 in silco-treated cylinders (stainless steel with inner surface coated with fused silica, Restek) and no issues with sample loss have been noticed. All collected samples were analysed by gas chromatography-mass spectrometry (GC-MS) at UEA, with a typical precision of 1-3 %.

Compared to other Cl-VSLS, scientific interest in DCE from an ozone depletion perspective is relatively new. As such, an international standard calibration scale has not yet been universally adopted across measuring groups. Historically, the scales

310 among the labs considered in this study have not differed by more than 10-30% for gases similar to DCE. However, in the absence of any formal assessment of calibration scale differences, an informal intercomparison for DCE was performed for this work. Background atmospheric DCE mole fractions from two remote sites (Barrow and Samoa Observatories), where both the NOAA and UCI groups sample, were compared (2017 – 2023). This intercomparison revealed an average offset of up to ~30% (UCI relatively high / NOAA relatively low), i.e. at the upper end of the above range. While this comparison is

315 limited in scope and will require further effort to refine (beyond the scope of this paper), this uncertainty is highlighted in the ensuing discussion.

Table 4. *Observed (Obs.) and modelled (Model) mean* ~~EDC~~ *DCE abundance (ppt) in the boundary layer (< 3 km) and in*

320 *different latitude bins during HIPPO and ATom. n denotes the number of measurements in each bin. Mean* ~~EDC~~ *DCE is reported with ±1 s.d. The mean bias (MB, model minus observation) is given for each bin. Model results are based on* ~~EDC~~ *DCE emission scenario sc05.*

Lat. Bin	HIPPO campaign				ATom campaign			
	n	*Obs.*	*Model*	*MB*	*n*	*Obs.*	*Model*	*MB*
>80°N	11	13.3 (±4.5)	12.6 (±4.7)	-0.7	2	17.7 (±2.6)	20.3 (±3.0)	2.6
60-80°N	77	14.8 (±4.5)	12.5 (±4.5)	-2.3	40	16.4 (±3.5)	19.3 (±4.0)	2.9
40-60°N	67	15.2 (±4.2)	13.0 (±4.7)	-2.2	55	17.3 (±5.9)	18.6 (±4.4)	1.3
20-40°N	53	15.9 (±6.7)	11.1 (±4.8)	4.8	28	16.4 (±8.3)	17.0 (±6.4)	0.7
0-20°N	49	8.5 (±3.7)	6.0 (±3.1)	-2.5	42	8.9 (±5.1)	7.5 (±4.2)	-1.3
0-20°S	40	3.5 (±1.2)	2.3 (±0.9)	-1.2	25	3.5 (±1.2)	2.7 (±0.7)	-0.7
20-40°S	68	1.9 (±0.5)	1.9 (±0.6)	0.02	21	1.9 (±0.3)	2.2 (±1.1)	0.3
40-60°S	36	1.9 (±0.4)	2.1 (±0.6)	0.2	35	1.8 (±0.3)	2.1 (±0.6)	0.4
≥60°S	12	1.8 (±0.4)	2.0 (±0.6)	0.2	22	1.7 (±0.2)	2.1 (±0.5)	0.4

3. Results and Discussion

3.1 Model-measurement comparison and emission constraint

325 Observed boundary layer ~~EDC~~ DCE mole fractions (<3 km), as averages from all deployments of HIPPO (2009-2011) and ATom (2016-2018), are shown in **Figure 3a** and **b**. The measurement data were compiled into 9 latitude bins (Section 2.4) and the mean (±1s.d.) of each bin is shown. Recall that both missions sampled air in various seasons of the year and thus the s.d. variability includes seasonal effects. Measurements from both missions show a strong hemispheric gradient, with mean NH mole fractions of ~15 ppt at latitudes greater than 40°N and ~4 ppt or less in the Southern Hemisphere (SH). For

330 comparison, ~~EDC~~ DCE mole fractions of 7.8 (±1.5) ppt have been previously reported in background air in the NH based on aircraft measurements from the 2006 NASA INTEX-B mission which sampled around the Gulf of Mexico and over the West Pacific off the US coast (Barletta et al., 2009; Singh et al., 2009). The data in **Figure 3** show that variability is large within the NH, where most ~~EDC~~ DCE production (and emission) is located and where the number of measurements is relatively large. For example, the relative standard deviation of the 20°-40°N bin is ~40% (HIPPO) and ~50% (ATom). For

335 comparison, the relative standard deviation in the SH is smaller; e.g. ~21% (HIPPO) and ~12% (ATom) for the <60°S bin.
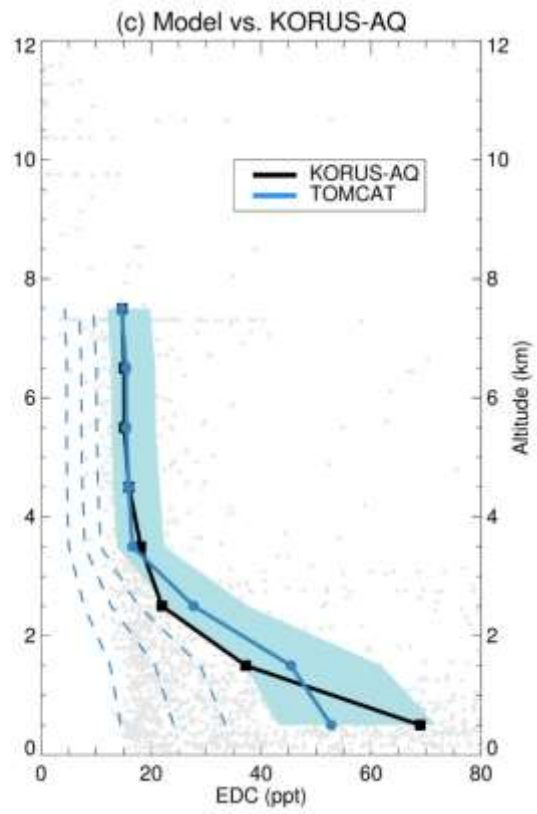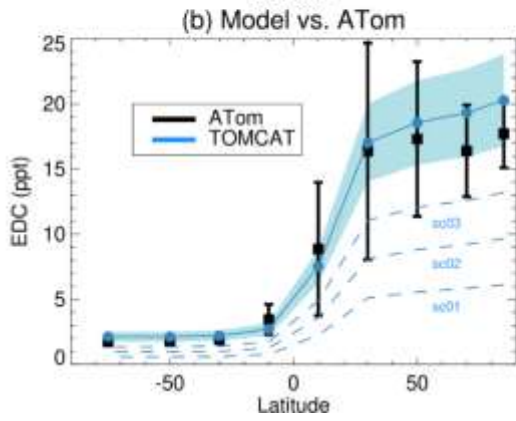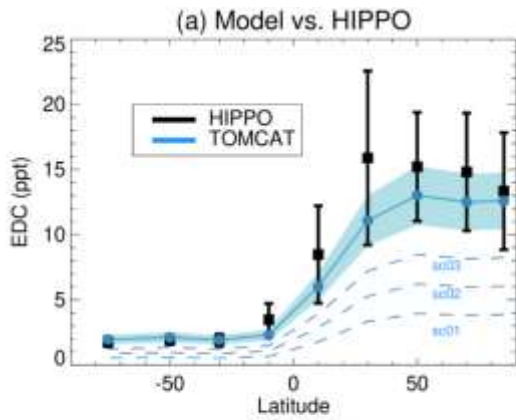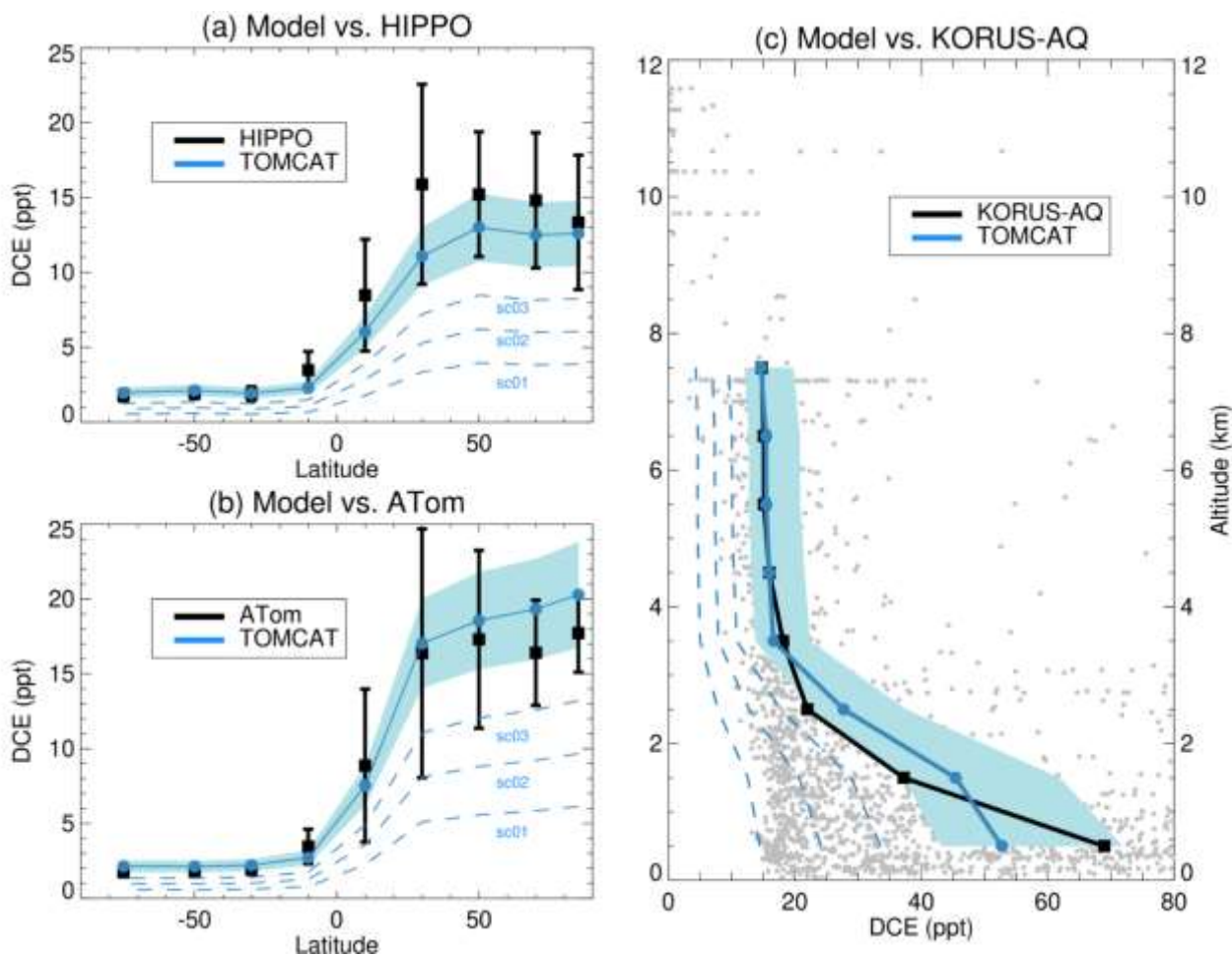
340

Figure 3. *(a-b) Observed* ~~EDC~~ *DCE mole fractions (ppt) as a function of latitude averaged over all deployments of each HIPPO (2009-2011) and ATom campaign (2016-2018). The data were obtained at < 3 km altitude and have been averaged in 9 latitude bins (see Section 2.4). Filled black symbols represent the mean within each bin (plotted at the central latitude) and error bars denote ±1s.d. The corresponding modelled* ~~EDC~~ *DCE abundance from TOMCAT is shown for different*
345 *assumed emission factors. Dashed lines denote scenarios sc01 through to sc03. The blue shaded region denotes the range obtained from sc04 to sc06 with the central sc05 case indicated (solid line). (c) Observed* ~~EDC~~ *DCE mole fractions vs altitude from the 2016 KORUS-AQ mission. All data from all flights (filled grey circles) were aggregated into 8 altitude bins (see Section 2.4) with the median of each bin shown (solid black line). Data points extend to 2.5 ppb but have been cut off at 80 ppt. The corresponding* ~~EDC~~ *DCE abundance from TOMCAT (also median) is shown as for other panels.*

350 **Figure 3** also includes the TOMCAT modelled ~~EDC~~ DCE abundance using the different emission scenarios, i.e. assuming different α_1 emission factors (see Section 2.2 and **Table 3**). With scenarios sc01 through to sc03 the model exhibits a substantial low bias and is unable to reproduce the magnitude of ~~EDC~~ DCE in either hemisphere or the observed

hemispheric gradient from each mission. Better model-measurement agreement for both missions is obtained from runs with scenarios sc04 through to sc06, shown by the shaded regions in **Figure 3**. The statistics describing model-measurement differences in **Table 4** are based on the central sc05 case, i.e. $\alpha_1 = 0.5\%$ (non-A5 countries) / 1.5% (A5). Under this scenario, the mean bias (model minus observation) varies by latitude and ranges from near zero up to 4.8 ppt. Although underestimating mean ~~EDC~~ DCE observed in the NH during HIPPO, the model falls within the measurement variability, and better agreement is obtained for the comparisons with ATom. Generally, model-measurement biases here are difficult to interpret and could in part reflect the model OH field (affecting the ~~EDC~~ DCE lifetime) and/or transport processes; they do not necessarily point to an under or overestimation of local emissions. Additionally, as for some other VSLS, differences in calibration scales between measurement groups (recall the discussion in Section 2.4) could be a confounding factor (see also Roozitalab et al., 2024 for a more detailed discussed). Importantly, model-measurement agreement is generally good in the tropics (±20° N/S), the region most relevant for diagnosing transport to the stratosphere, throughout the vertical profile (see Supplement **Figure S1**). The low abundance of DCE ~~EDC~~ at SH high latitudes is also well captured.

A comparison of the modelled vertical profile of ~~EDC~~ DCE to that observed during KORUS-AQ (2016) is shown in **Figure 3c**. Compared to HIPPO and ATom, far larger observed levels of EDC are apparent at lower altitudes (up to 2.5 ppbv; not shown in Figure 3c), along with very large variability (see filled grey circles). To accommodate the latter, binned measurement data in **Figure 3c** show the median as opposed to the mean and the horizontal axis is capped at 80 ppt (note, a version of this comparison but with the means is shown in **Figure S2**). The maximum observed value of >2.5 ppb occurred in the 0-1 km bin for air originating from China. A similar maximum of >2.4 ppb was measured in air originating from an industrial facility in South Korea (Simpson et al., 2020), though we note that a global scale model is not expected to capture these most extreme values, which included targeted source sampling. Although the model (median ~53 ppt under scenario sc05) underestimates the observations (median ~69 ppt) in the lowest bin (0-1 km), it is evident from comparing **Figure 3c** with **3a** and **3b** that the model shows significantly elevated ~~EDC~~ DCE in this region. Elevated emissions over East Asia are also a clear feature in Figure 2a. Above 1 km, there is very close agreement between the model and measurements using scenario sc05. A full quantitative comparison is given in **Table S2** in the Supplement. A previous in-depth analysis of the KORUS-AQ data highlighted that ~~EDC~~ DCE was especially elevated in air originating from China (Simpson et al., 2020). Similarly, during the 2006 NASA INTEX-B mission, analysis of air sampled in polluted plumes from Asia (though especially China) revealed substantially elevated ~~EDC~~ DCE relative to background air and to plumes from the USA (Barletta et al., 2009). Indeed, ~~EDC~~ DCE was used as a tracer of air from China during both INTEX-B and KORUS-AQ.

The modelled ~~EDC~~ DCE abundance is compared to the available surface measurements from Bachok and Taiwan in **Figure 4**. As above, the measurements are characterised by large variability with ~~EDC~~ DCE exceeding 150 ppt at Bachok and 300 ppt at Taiwan on some days. While the model is not expected to capture the most extreme values, the central tendency of the observations appears to be reasonably well captured at both sites under scenario sc05 (see **Table S1** in Supplement). Both the measurements and model show especially elevated levels of ~~EDC~~ DCE at Taiwan (median values >50 ppt in each year of

sampling) with respect to levels observed during HIPPO and ATom, suggesting strong regional or local sources and sampling of relatively polluted air in both the Bachok and Taiwanese samples. Samples collected at Bachok, where the model captures the shape of the seasonal cycle well, predominately occur when the site experiences north-easterly winds and observations are thus likely impacted by emissions occurring from mainland China (Oram et al. 2017). This seasonality is

390   discussed in, for example, Oram et al. (2017) and has a large dynamical component. Briefly, strong north-easterly (NE) winds that form in NH winter transport polluted airmasses from continental East Asia deep into the tropics. The prevailing NE winds may also be strengthened during 'cold surge' events. The effect of such events on various tracers have been observed, including at other sites in Malaysia (e.g., Ashfold et al. 2015, 2017). Similarly, owing to the close proximity, measurements at Taiwan are expected to be influenced by emissions from mainland China. Although not exhaustive, these

395   comparisons discussed above (along with those for KORUS-AQ above) suggest the model has a reasonable representation of regional emissions in East and South East Asia. Note, at Taiwan (only) the modelled EDC DCE abundance was found to exhibit a strong sensitivity to the choice of model vertical level sampled. Model data in **Figure 4b** therefore represent the average of the two model levels closest to the surface.

400
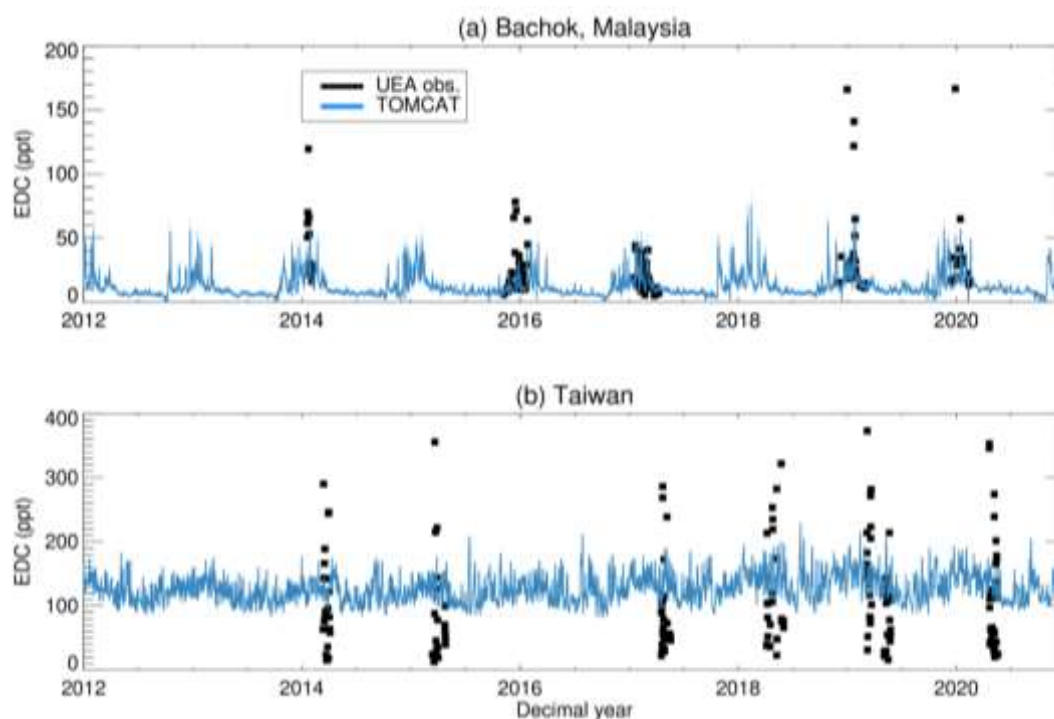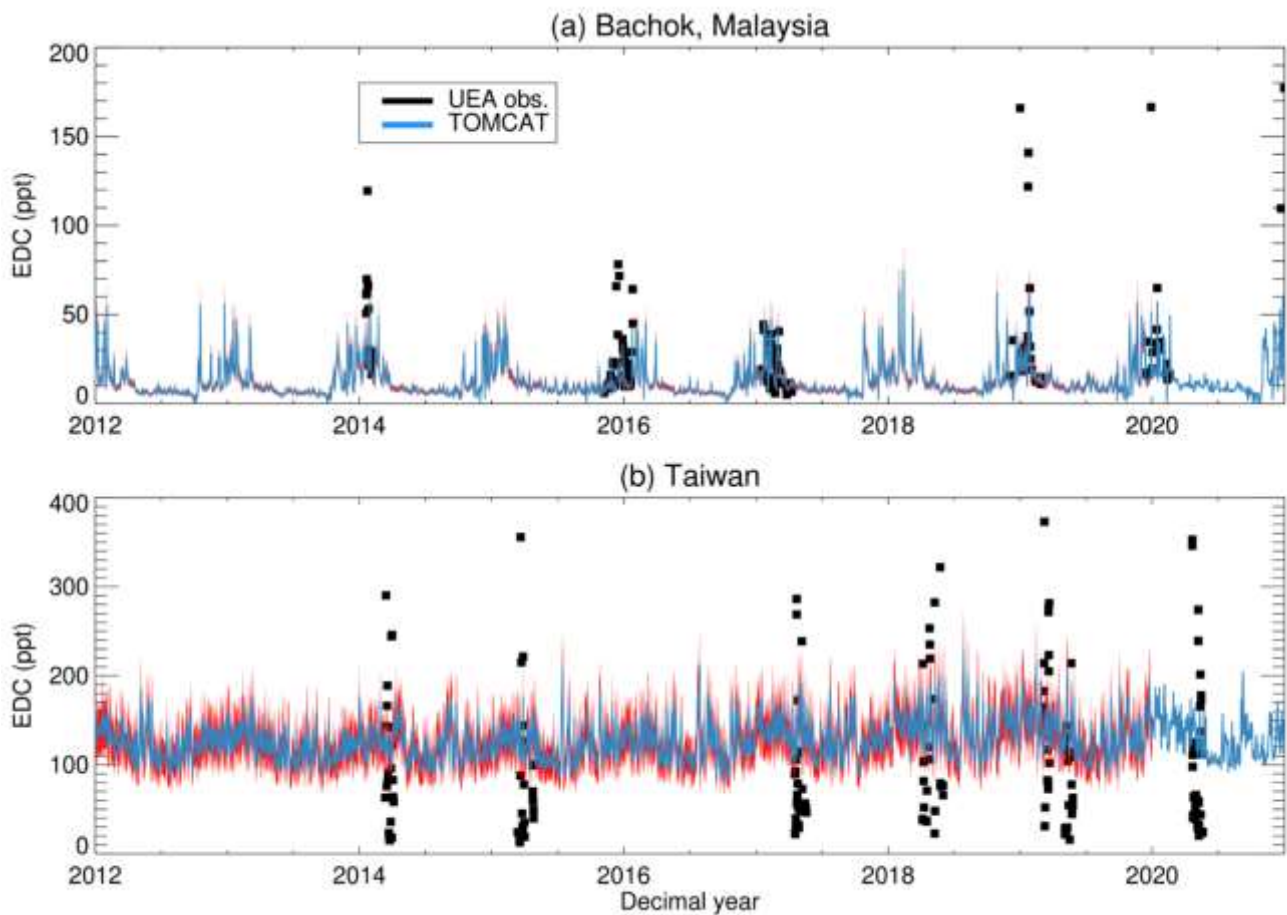
Figure 4. *Observed ~~EDC~~ DCE surface mole fraction (ppt) at (a) Bachok and (b) Taiwan. The corresponding modelled ~~EDC~~ DCE abundance from TOMCAT (sampled daily) is shown for scenario sc05, with ~~blue shaded regions denoting~~ the range from scenarios sc04 and sc06 shown in red for clarity.*

Although the regional variability of atmospheric ~~EDC~~ DCE measurements can be large, the remote atmospheric survey sampling represented by the HIPPO and ATom missions, along with the other comparisons, allows for some constraint on the global ~~EDC~~ DCE source (given our assumptions concerning the ~~EDC~~ DCE emission distribution). Assuming scenario sc05, $\alpha_1 = 0.5\%$ (non-A5 countries) / 1.5 % (A5 countries), shown above to provide reasonable model-measurement agreement, we estimate a global ~~EDC~~ DCE source of 349 (±61) Gg/yr in 2002, rising to 505 (±90) Gg/yr in 2020 (i.e. an increase of ~45%). The mean growth rate of global DCE emissions over this period is ~9.1 Gg/yr^2. There are very few estimates of global or regional ~~EDC~~ DCE emissions in the literature with which to compare these findings. Using a simple

tracer ratio method, Wang et al. (2014) estimated Chinese ~~EDC~~ DCE emissions of 121.6 (±89) Gg/yr in 2010. For the same

415 year and again utilising scenario sc05 (range sc04 to sc06), our inventory produces significantly lower Chinese ~~EDC~~ DCE emissions of ~44 (36-52) Gg/yr. Oram et al. (2017) estimated Chinese ~~EDC~~ DCE emissions of 203 (±9) Gg/yr for 2015 based on measurements obtained in Taiwan and Malaysia. Our estimate for Chinese emissions in 2016 is ~60 (49-71) Gg/yr and is thus substantially lower. However, it should be emphasised that inferred emissions from observed tracer correlations, as in the above studies, are based on several assumptions and subject to large uncertainty. For instance, emissions occurring

420 in nearby regions may confound geographical attribution. Although still lower, our inventory provides better agreement to the above estimates if emissions from, for instance, nearby Taiwan are included. We estimate the sum of ~~EDC~~ DCE emissions from China and Taiwan to be 89 (73-106) Gg in 2010 and 107 (87-127) Gg in 2016. A summary of these comparisons of Chinese emissions is given in **Table S3** of the Supplement. A further factor that may confound the comparison of these different estimates is the month of measurement and sampling frequency used to infer tracer ratios. For

425 example, note that the ~~EDC~~ DCE measurements at Bachok reported by Oram et al. (2017), an extended timeseries of which are shown in **Figure 4a**, focus on non-summer months when ~~EDC~~ DCE is relatively abundant at that site.

While the above results provide some constraint on the global ~~EDC~~ DCE source required to reproduce atmospheric observations, some care is needed when interpreting the findings from an emission process standpoint. Our analysis has approximated fugitive emissions arising from production, feedstock use and distribution, assuming feedstock uses account

430 for all consumption in every country. However, ~~EDC~~ DCE has known solvent uses (not explicitly accounted for) which may be up to 100% emissive in the absence of solvent capture and careful disposal. If a non-negligible amount of the observed atmospheric abundance of ~~EDC~~ DCE stems from solvent use, then the contribution from fugitive losses could be overestimated. We anticipate that ~~EDC~~ DCE solvent use is most prevalent in developing countries where it is relatively cheap versus alternatives and is readily available, and where concerns over its toxicity may not yet have resulted in

435 restrictions on its use. Given these uncertainties, we do not overinterpret our findings from an emission process or sectoral standpoint but rather, with more confidence, highlight the overall magnitude of emissions that provide good agreement with the available measurement data in **Figure 3**. In subsequent sections, we present all model quantities assuming scenario sc05 emissions, with reported uncertainties from the sc04 and sc06 cases.

3.2 Lifetime, tropospheric distribution, and contribution to stratospheric chlorine

440 The modelled tropospheric distribution of ~~EDC~~ DCE is shown in **Figure 5** for the years 2002 and 2020. At the surface (panels a and b) ~~EDC~~ DCE exhibits large spatial variability and has a strong hemispheric gradient. Hotspots occur within the industrialised zones of its main source regions (USA, Europe, East Asia). Recall, the ~~EDC~~ DCE emission distribution within countries is prescribed here to follow that of ethene. In reality, the ~~EDC~~ DCE source may be less dispersed than assumed, particularly if fugitive emissions occur from a relatively small number of point plant locations. Growth in the NH

445 background of ~~EDC~~ DCE is apparent from **Figure 5** and we estimate that the global EDC burden increased from ~81 (±15)

Gg to ~116 (±21) Gg between 2002 and 2020 (**Table 5**). Chemical loss of ~~EDC~~ DCE is controlled primarily through reaction with OH and we calculate an overall global ~~EDC~~ DCE lifetime, defined as the ratio of its global burden over its global loss rate, to be ~83 days in 2020 (**Table 5**). This is in very close agreement to the ~82 days reported by Burkholder and Hodnebrog (2022).

450 It is well established that VSLS may contribute to stratospheric halogen loading via both source gas injection (SGI) and product gas injection (PGI). Chlorine SGI and PGI from ~~EDC~~ DCE are also shown in **Figure 5**. Defining these quantities at the tropical tropopause (~17 km), the total (SGI+PGI) stratospheric chlorine input from EDC in the year 2020 is estimated to be 12.9 (±2.4) ppt Cl, comprising 10.7 (±2) ppt Cl from SGI and 2.2 (±0.4) ppt Cl from PGI (**Table 5**). For context, the total Cl-VSLS supply to the stratosphere (including VSLS other than ~~EDC~~DCE) was estimated to be ~130 (100-160) ppt Cl in 455 2019 when total stratospheric chlorine (i.e. including long-lived gases) was around 3240 ppt Cl (Laube and Tegtmeier et al., 2020). Our ~~EDC~~ DCE SGI estimate in 2020 is similar to the 8.5 (±1.9) ppt Cl reported in our previous modelling work (that did not include geographically- or time-varying emissions) for the year 2017 (Hossaini et al., 2019). A notable difference with our previous work is that here we assess that stratospheric chlorine from ~~EDC~~ DCE has increased significantly over time (see **Figure S2~~2~~3**), reflecting growth in emissions and hence SGI. Based on an ordinary least square regression applied 460 to the model output over the full study period (2002 to 2020, **Figure S3**), mean growth rates for SGI and PGI are 0.19 ppt Cl/yr and 0.04 ppt Cl/yr, respectively.

In the current study, our estimated chlorine PGI is also similar to the value of ~2 ppt Cl reported in Hossaini et al. (2019). The latter assumed a fixed lifetime of Cl$_y$ in the troposphere against deposition (~5 days), while here we adopted an improved, more explicit representation in which Cl$_y$ washout was calculated using the standard TOMCAT deposition 465 routines for the component chlorine species (Section 2.3). As for all VSLS, lack of observational constraint means that modelled PGI estimates carry significant uncertainty. A process not considered here is the heterogeneous recycling of Cl$_y$ on ice crystals in the upper troposphere, for which there is some observational evidence (von Hobe et al., 2011). As demonstrated for iodine (Saiz-Lopez et al., 2015), such a process could plausibly extend the Cl$_y$ lifetime and thus increase the magnitude of PGI. However, note that the net effect on PGI will likely depend on the interplay between ice-uptake 470 followed by sedimentation and also heterogeneous ice-recycling reactions that return species back to the gas phase (e.g. Fernandez et al., 2014; 2020). Such processes and the required parameters with which to treat them in a global model are highly uncertain.

The model estimates of chlorine SGI from ~~EDC~~ DCE that are presented in **Figure 5** (c and d) and **Table 5** are annual mean quantities at the tropical tropopause, averaged zonally over the whole of the tropics (±20°N/S). While transport across the 475 tropical tropopause is the main route via which air enters the stratosphere, relatively elevated levels of VSLS (and other gases) have been reported in the subtropical NH lower stratosphere owing to the effects of the Asian summer monsoon (ASM) and ASM anticyclone (e.g. Fiehn et al., 2017; Keber et al., 2020; Lauther et al., 2022). Forming in boreal summer, ASM dynamics are characterised by rapid uplift of boundary layer air to the UTLS by deep convection (e.g. Randel and

Park, 2006; Basha et al., 2020), including relatively polluted air masses from South and East Asia (e.g. Li et al., 2005;
480   Randel et al., 2010; Müller et al. 2016). Based on aircraft measurements obtained during the Asian Monsoon Anticyclone
2017 campaign (AMA-17) over the Indian subcontinent, Adcock et al. (2021) reported a mean ~~EDC~~ DCE mole fraction
around the tropopause (355-375 K) of ~12 ppt (with a range of 4.5 to 23 ppt), corresponding to a chlorine SGI (i.e. 2× the
~~EDC~~ DCE mole fraction) in the range 9-47 ppt Cl. The AMA-17 measurements were obtained in July and August in the
latitude range 21°N-29°N, longitude range 79°E-91°E, and from ~10-20 km altitude. The measurements from Adcock et al.
485   (2021) are shown in **Figure S~~3~~4** of the Supplement along with corresponding model estimates. There is generally good
agreement between the two datasets and the model corroborates the signal of relatively large levels of ~~EDC~~ DCE around the
tropopause (~10 ppt) and hence a larger local stratospheric chlorine SGI (~20 ppt Cl) in this region/season relative to the
annual mean quantities around the tropical tropopause reported in **Table 5**.
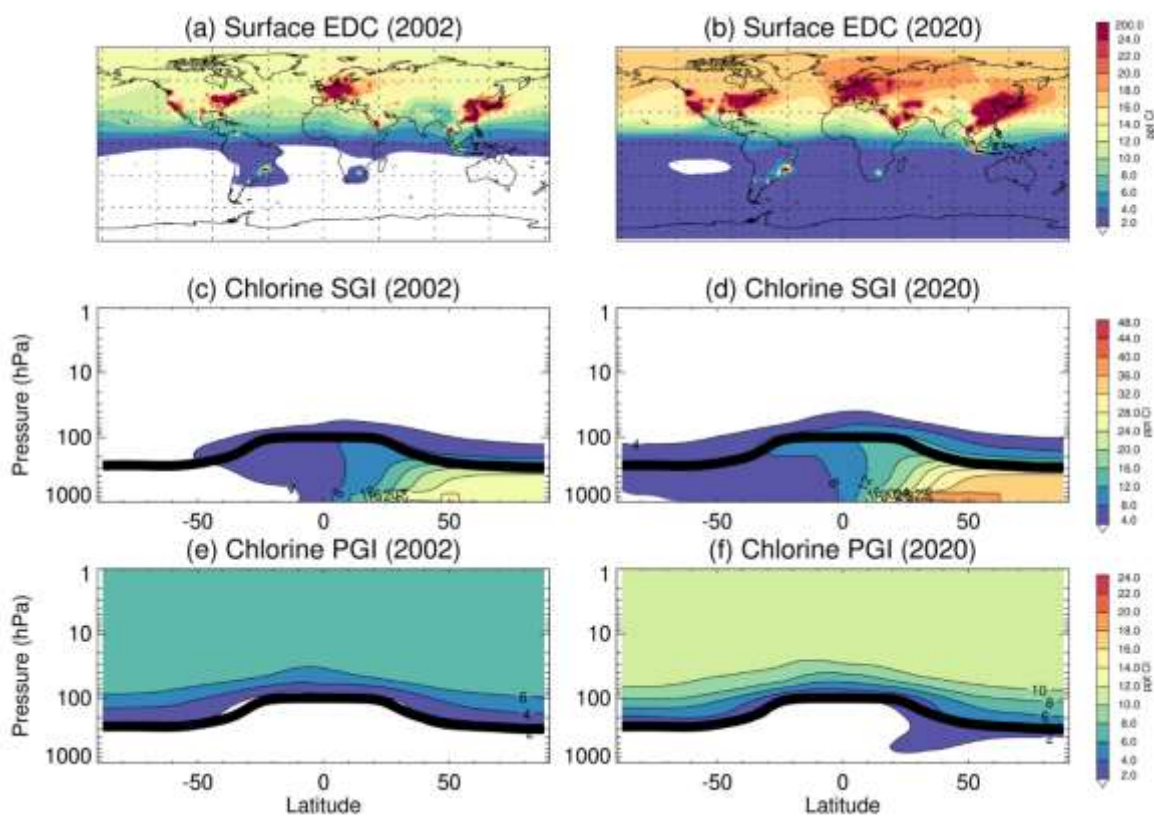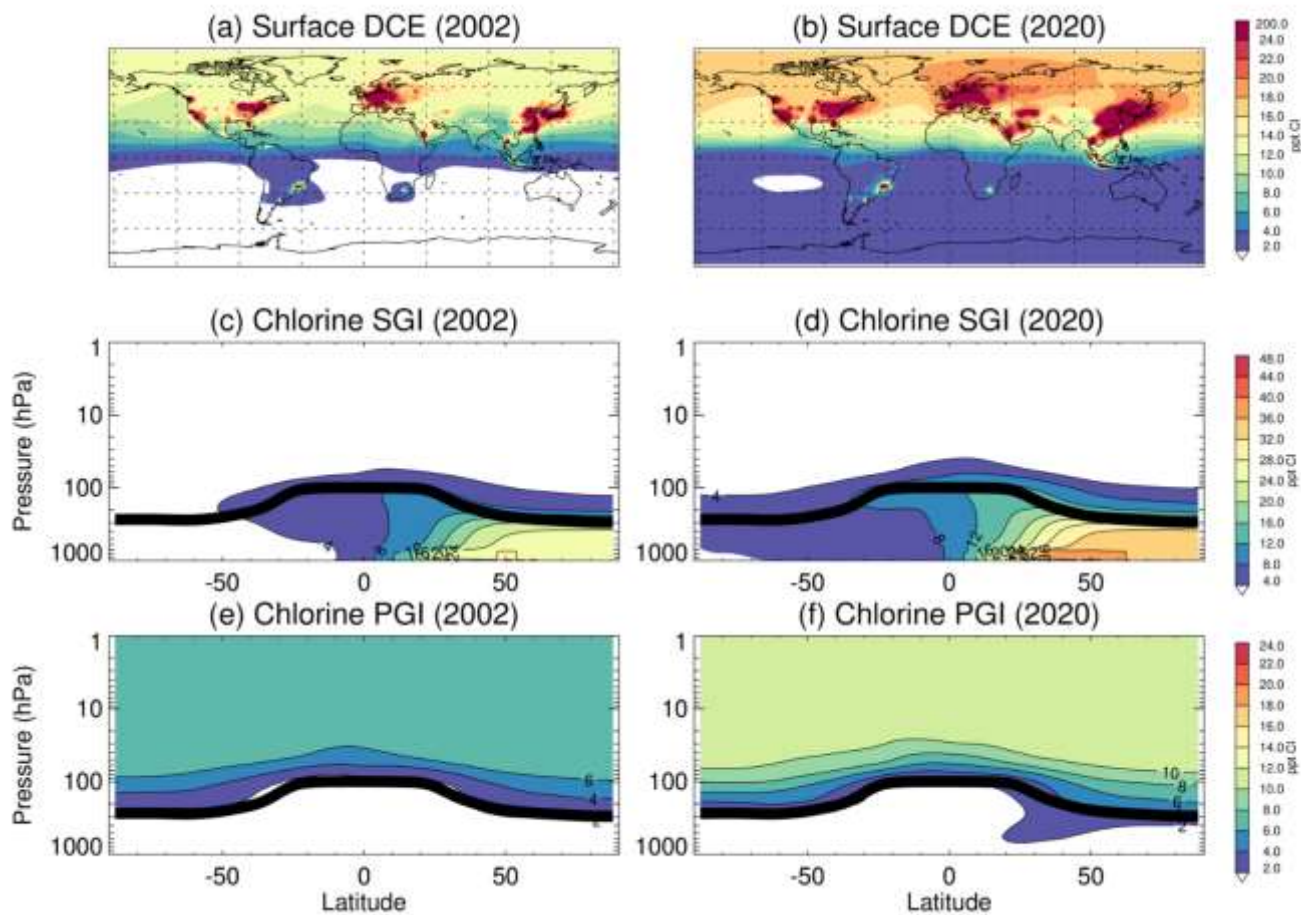
490

Figure 5. *Modelled annual mean ~~EDC~~ DCE volume mixing ratio (ppt) at the surface under scenario sc05 in (a) 2002 and (b) 2020. Panels (c-d) show the latitude-pressure distribution of chlorine SGI from ~~EDC~~ DCE (ppt Cl) for the same years. Panels (e-f) show chlorine PGI from ~~EDC~~ DCE (ppt Cl). The thermal tropopause pressure based on ERA5 reanalysis (Hoffmann and Spang, 2022) is shown by the black line.*

495

Table 5. *Modelled ~~EDC~~ DCE burden (total mass), global loss rate (due to OH), overall global lifetime (burden / loss rate) and contribution to stratospheric chlorine (ppt Cl) through SGI, PGI and total (SGI + PGI). All fields are annual averages for the years 2002 or 2020 and results are shown for emission scenarios (sc) sc04, sc05 and sc06.*

Sc	Burden (Gg)		Loss rate (Gg/yr)		Lifetime (days)		SGI (ppt Cl)		PGI (ppt Cl)		Total Cl (ppt Cl)	
	2002	*2020*	*2002*	*2020*	*2002*	*2020*	*2002*	*2020*	*2002*	*2020*	*2002*	*2020*
04	67	95	289	417	85	83	5.5	8.8	1.2	1.8	6.7	10.6

| 05 | 81 | 116 | 350 | 508 | 85 | 83 | 6.7 | 10.7 | 1.5 | 2.2 | 8.2 | 12.9 |
| 06 | 96 | 137 | 411 | 598 | 85 | 83 | 7.9 | 12.7 | 1.7 | 2.6 | 9.6 | 15.3 |

Other recent studies have also highlighted the importance of Asian emissions in contributing to the atmospheric loading of a range of Cl-VSLS. For example, in a global modelling study, Roozitalab et al. (2024) used a 'tagged tracer' approach to show that Asian emissions likely dominate the global CH_2Cl_2 and C_2Cl_4 distribution. This was the case not only at the surface but also at high altitudes (150 hPa). The same study also analysed measurements of several Cl-VSLS (including DCE) during the ATom campaign and tentatively assigned relatively enhanced NH mid-latitude mole fractions of Cl-VSLS (observed during ATom-1) as being influenced by deep convection associated with the Asian Summer Monsoon. High-altitude aircraft observations from the ACCLIP mission have also revealed that the lower stratospheric abundance of Cl-VSLS above the East Asian monsoon are at least a factor of 2 larger than previously observed in the tropics (Pan et al., 2024).

3.3 Impact of ~~EDC~~ DCE emissions on ozone

The modelled stratospheric ozone change due to ~~EDC~~ DCE under 2020 conditions is shown in **Figure 6**. ~~EDC~~ DCE decreases stratospheric ozone globally, though the effect is generally small. The largest absolute decreases occur in the upper stratosphere (10-1 hPa) and polar lower stratosphere (200-20 hPa), i.e. regions where chlorine-catalysed ozone loss is known to be important (e.g. Chipperfield et al., 2018). The absolute ozone decreases in **Figure 6** (panels a-b) are up to ~5 ppb when expressed as an annual average (panel a). Larger decreases (up to ~10 ppb) occur within SH high latitudes in Spring when the Antarctic ozone hole forms (panel b). Corresponding ozone changes expressed in percent are shown in panels c-d. In most regions, the ozone changes due to ~~EDC~~ DCE represent changes of <1%, though in the SH polar spring reductions of up to ~1.3% in the lower stratosphere are found.

The small (though non-zero) effect of ~~EDC~~ DCE on global stratospheric ozone reflects the relatively small input of chlorine from EDC to the stratosphere (see above). However, as noted ~~above~~, several studies have identified transport via the ASM as a route through which relatively large local injections of various VSLS (including ~~EDC~~DCE) to the extratropical lower stratosphere can occur (Keber et al., 2020; Adcock et al., 2021; Lauther et al., 2022; Pan et al., 2024). In principle, this process and its effect on chlorine injection from ~~EDC~~ DCE is represented in our model (see **Figure S~~3~~4**). However, the very large surface levels of ~~EDC~~DCE, in at least some parts of Asia (see **Figure ~~2~~3c**), that are not tightly constrained by the data considered here may be underestimated in this analysis and thus too the co-location of emission hotspots with regions of relatively fast vertical ascent. Nonetheless, the local impact of DCE on summertime stratospheric ozone in the ASM region was briefly examined and is shown in **Figure S5**. Noting again that chlorine-catalysed ozone destruction is generally efficient in the polar lower stratosphere and upper stratosphere, we find that ozone changes due to DCE in the lower stratosphere above the ASM region/season (i.e. the localised effect) are small (<0.1%). Ultimately, ~~T~~the overall significance of the Asian Summer Monsoon transport pathway for VSLS-driven stratospheric ozone loss is an area of current research

and will require further and more detailed investigation that considers other VSLS species (including those with predominately natural sources) and would benefit once from new measurements in this region become available.

This study has focussed only on the possible direct impact of EDC DCE emissions on ozone. However, we note that a broader impact assessment (beyond the scope of this work) might also factor in the unintended, but expected to be very minor, formation of other halogenated chemicals that inevitably occur during the EDC DCE production process (the majority of such are destroyed by thermal oxidation or other means). These species are found in the "lights" and "heavies" effluent streams which may range from 0.3-1.0% of the EDC DCE produced (TEAP, 2022), and which include a proportion of ODSs, such as carbon tetrachloride (CCl_4), and other chlorinated VSLS, such as chloroform ($CHCl_3$).
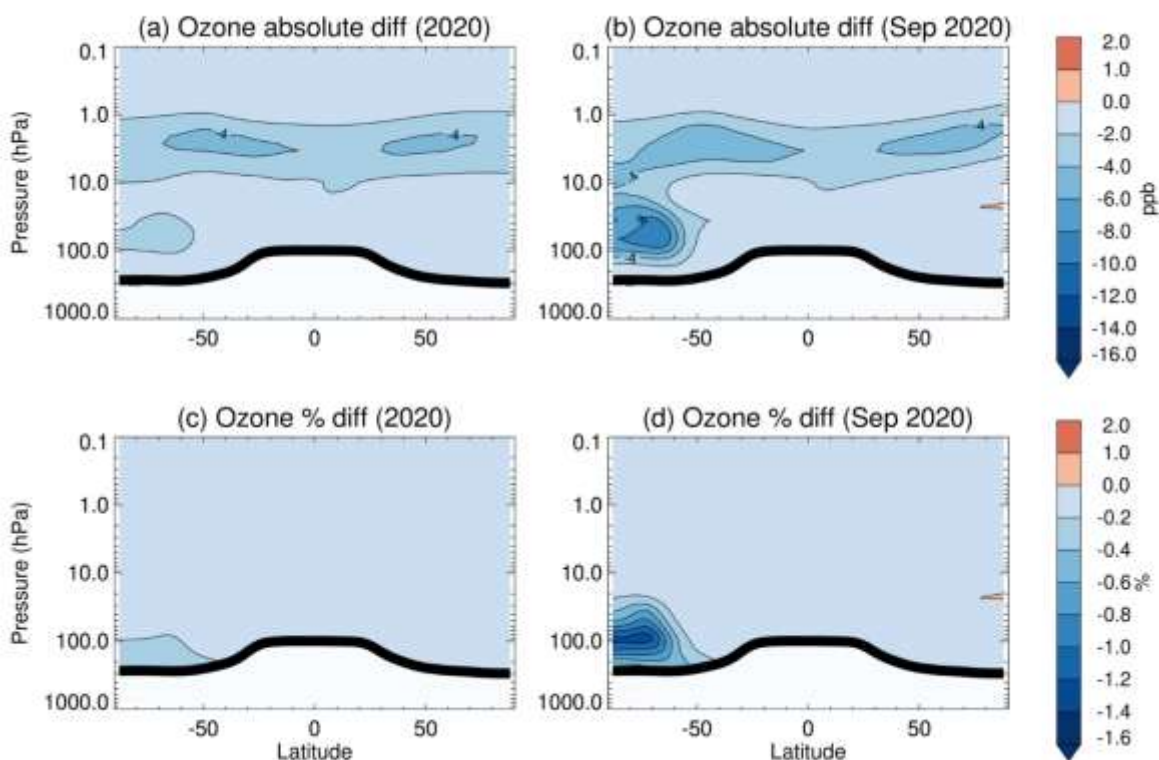
Figure 6. *Modelled stratospheric ozone decrease due to EDC DCE in 2020 expressed as (a,c) an annual average, and (b,d) September average (i.e. Antarctic ozone hole season). Panels (a-b) show absolute decreases (ppb) and panels (c-d) percentages. Model results calculated based on the difference between simulations with EDC DCE (scenario sc05) and without EDCDCE.*

4. Summary and concluding remarks

The global production of ~~EDC~~ DCE in the year 2020 exceeded 50 million tons. However, despite annual production volume greatly exceeding that of other more prominent industrial VSLS (e.g. CH_2Cl_2, $CHCl_3$), few atmospheric observations of EDC exist and little is known of its global budget. In this study, we combined information on industrial ~~EDC~~ DCE production, trade statistics, and assumptions on its fugitive losses, to explore the plausible range of global ~~EDC~~ DCE emissions. Time-varying gridded ~~EDC~~ DCE emission fields were developed using a bottom-up approach and then included in the TOMCAT CTM. Transient simulations were performed to assess the ~~EDC~~ DCE source required to reproduce a variety of measurements from recent aircraft missions (HIPPO, ATom, and KORUS-AQ) and from ground sites in South East Asia. Based on constraints provided by these comparisons, we infer a global ~~EDC~~ DCE source of 349 (±61) Gg/yr in 2002, rising to 505 (±90) Gg/yr in 2020 (i.e. an increase of ~45%). Our framework for calculating ~~EDC~~ DCE emissions assumed that all releases to the atmosphere result from fugitive losses during its production, its use as a feedstock (largely to produce VCM in the PVC production chain), and during its supply chain. Reasonably good agreement between the model and ~~EDC~~ DCE observations is achieved assuming a production emission factor of ~0.5% in developed countries and 1.5% in developing countries. These factors are within the generic 'most likely' range of factors (0.9-4.0%) applicable to a range of other gases assessed by TEAP (2022). Large uncertainty around the magnitude and emissions associated with ~~EDC~~ DCE solvent use, which is potentially widespread in developing countries and East Asia, is a confounding factor in our analysis and prevents firm conclusions as to the specific sectors contributing to the observed ~~EDC~~ DCE signal and the global distribution of these emissions.

We estimate that ~~EDC~~ DCE contributed 12.9 (±2.4) ppt of chlorine to the stratosphere in 2020. Based on this loading, we estimate ~~EDC~~ DCE decreased ozone by up to several ppb in 2020, with the largest changes occurring in the upper stratosphere and high-latitude lower stratosphere. Outside of the SH lower stratosphere in Spring, where the ozone decreases attributable to ~~EDC~~ DCE are up to ~1.3%, the effect of ~~EDC~~ DCE on global stratospheric ozone is presently small (<1%), though non-zero. Any future growth in EDC emissions (e.g. tied to downstream demand for PVC) may increase the contribution of ~~EDC~~ DCE to stratospheric chlorine and thereby increase its impact on ozone. Such possible future effects would need to be examined with knowledge of the global PVC market and its possible future trajectories and an assessment of use and emissions from the ~~EDC~~ DCE solvent sector. Diagnosing future changes in the contribution of ~~EDC~~ DCE to ozone-depleting chlorine in the stratosphere would also benefit from routine observations of ~~EDC~~ DCE at sites across the globe.

Data availability

The TOMCAT model output and gridded emission data will be uploaded to the Zenodo open access repository (https://zenodo.org/) or similar if the manuscript is accepted for publication following peer-review.

Author contribution

RH conceived and led the study and developed the emission inventories in collaboration with~~,~~ and based on data~~.~~ ~~and~~ analysis and advice provided by~~,~~ DS. ZW performed the TOMCAT/SLIMCAT model simulations supervised by MPC and WF. AM and AL contributed to the analysis of model output. DO, KA, CC, SAM, IJS and EA provided atmospheric measurements and interpretation of these data. RH prepared the original draft of the paper. All authors contributed to reviewing and editing of the manuscript.

Competing interests

The authors declare that they have no conflict of interest.

Acknowledgements

RH, MPC and WF were supported by the NERC projects LSO3 (NE/V011863/1) and InHALE (NE/X003582/1). UEA would like to thank Lauren Gooch and Debbie Sanchez for past assistance with sample analysis and Ahmad Amin Abdullah for sample collection at the Bachok Marine Research Station. The long-term sampling programmes in Taiwan and Malaysia were established through the NERC International Opportunities fund (NE/J016012/1, NE/N006836/1) and subsequently supported through the NERC SISLAC (NE/R001782/1) and LSO3 (NE/V011863/1) projects. K.E.A. was funded by the UK Natural Environment Research Council through the EnvEast Doctoral Training Partnership (Grant NE/L002582/1). SAM acknowledges the assistance of those facilitating measurements and calibration scales at NOAA including B. Hall, F. Moore, K. McKain, and C. Siso. EA acknowledges technical assistance from X. Zhu and L. Pope and financial support from NASA grant #80NSSC22K1284 and NSF AGS grants #0959853 and #1853948.

References

Adcock, K. E., Fraser, P. J., Hall, B. D., Langenfelds, R. L., Lee, G., Montzka, S. A., Oram, D. E., Röckmann, T., Stroh, F., Sturges, W. T., Vogel, B., and Laube, J. C.: Aircraft-Based Observations of Ozone-Depleting Substances in the Upper Troposphere and Lower Stratosphere in and Above the Asian Summer Monsoon, J. Geophys. Res.-Atmos., 126, e2020JD033137, doi.org/10.1029/2020jd033137, 2021

An, M., Western, L.M., Say, D., Chen, L., Claxton, T., Ganesan, A.L., Hossaini, R., Krummel, P.B., Manning, A.J., Mühle, J., O'Doherty, S., Prinn, R.G., Weiss, R.F., Young, D., Hu, J., Yao, B., and Rigby, R.: Rapid increase in dichloromethane emissions from China inferred through atmospheric observations. Nat Commun., 12, 7279, 2021.

An, M., Western, L.M., Hu, J., Yao., B., Mühle, J., Ganesan, A.L., Prinn, R.G., Krummel, P.B., Hossaini, R., Fang, X., O'Doherty, S., Weiss, R.F., Young, D., and Rigby, M.: Anthropogenic Chloroform Emissions from China Drive Changes in Global Emissions, Environ. Sci. Technol., 57, 13925–13936, doi.org/10.1021/acs.est.3c01898, 2023.

605 Ashfold, M. J., Pyle, J. A., Robinson, A. D., Meneguz, E., Nadzir, M. S. M., Phang, S. M., Samah, A. A., Ong, S., Ung, H. E., Peng, L. K., Yong, S. E., and Harris, N. R. P.: Rapid transport of East Asian pollution to the deep tropics, Atmos. Chem. Phys., 15, 3565–3573, doi.org/10.5194/acp-15-3565-2015, 2015.

Ashfold, M.J. Latif, M.T., Samah, A.A., Mead, M.I., and Harris, N.R.P.: Influence of Northeast Monsoon cold surges on air quality in Southeast Asia, Atmos. Env., 166, 498-509, doi.org/10.1016/j.atmosenv.2017.07.047, 2017.

ATSDR (Agency for Toxic Substances and Disease Registry): Toxicological Profile for 1,2-Dichloroethane (Draft for Public 610 Comment). Chapter 5 (Potential For Human Exposure). Atlanta, GA, U.S. Department of Health and Human Services, Public Health Service, 2022.

Ayres, R.U. and Ayres, L.W.: The Life Cycle of Chlorine, Part II: Conversion Processes and Use in the European Chemical Industry. Journal of Industrial Ecology, 1, 65-89, doi.org/10.1162/jiec.1997.1.2.65, 1997.

Basha, G., Ratnam, M. V., and Kishore, P.: Asian summer monsoon anticyclone: trends and variability, Atmos. Chem. 615 Phys., 20, 6789–6801, doi.org/10.5194/acp-20-6789-2020, 2020.

Barletta, B., Meinardi, S., Simpson, I. J., Atlas, E. L., Beyersdorf, A. J., Baker, A. K., Blake, N. J., Yang, M., Midyett, J. R., Novak, B. J., McKeachie, R. J., Fuelberg, H. E., Sachse, G. W., Avery, M. A., Campos, T., Weinheimer, A. J., Rowland, F. S., and Blake, D. R.: Characterization of volatile organic compounds (VOCs) in Asian and north American pollution plumes during INTEX-B: identification of specific Chinese air mass tracers, Atmos. Chem. Phys., 9, 5371–5388, 620 doi.org/10.5194/acp-9-5371-2009, 2009.

Bednarz, E. M., Hossaini, R., Chipperfield, M. P., Abraham, N. L., and Braesicke, P.: Atmospheric impacts of chlorinated very short-lived substances over the recent past – Part 1: Stratospheric chlorine budget and the role of transport, Atmos. Chem. Phys., 22, 10657–10676, doi.org/10.5194/acp-22-10657-2022, 2022.

Bednarz, E. M., Hossaini, R., and Chipperfield, M. P.: Atmospheric impacts of chlorinated very short-lived substances over 625 the recent past – Part 2: Impacts on ozone, EGUsphere [preprint], doi.org/10.5194/egusphere-2023-496, 2023.

Burkholder, J. B., Sander, S. P., Abbatt, J., Barker, J. R., Cappa, C., Crounse, J. D., Dibble, T. S.and Huie, R. E., Kolb, C. E., Kurylo, M. J., Orkin, V. L., Percival, C. J., Wilmouth, D. M., and Wine, P. H.: Chemical Kinetics and Photochemical Data for Use in Atmospheric Studies, Evaluation No. 19, Tech. rep., JPL Publication 19-5, Jet Propulsion Laboratory, Pasadena, 2019.

Burkholder, J.B., and Hodnebrog, Ø.: Summary of Abundances, Lifetimes, ODPs, REs, GWPs, and GTPs. In Scientific assessment of ozone depletion: 2022, GAW Report No. 278, Annex. World Meteorological Organization, Geneva, Switzerland, 2022.

CEH (Chemical Economics Handbook), 2023. https://www.spglobal.com/commodityinsights/en/ci/products/ethylene-dichloride-chemical-economics-handbook.html

Cherrie, J.W., Gorman, M., Shafrir, A., van Tongeren, M., Mistry, M., Sobey, M., Corden, C., Rushton, L., and Hutchings, S.: Health, socio-economic and environmental aspects of possible amendments to the EU Directive on the protection of workers from the risks related to exposure to carcinogens and mutagens at work, IOM Research Project, SHEcan Report P937/17, 2011.

Chipperfield, M. P.: New version of the TOMCAT/SLIMCAT offline chemical transport model: intercomparison of stratospheric tracer experiments, Q. J. Roy. Meteor. Soc., 132, 1179–1203, doi:10.1256/qj.05.51, 2006.

Chipperfield, M. P., Dhomse, S., Hossaini, R., Feng, W., Santee, M. L., Weber, M., Burrows, J. P., Wild, J. D., Loyola, D., and Coldewey-Egbers, M.: On the cause of recent variations in lower stratospheric ozone, Geophys. Res. Lett., 45, 5718–5726, doi.org/10.1029/2018GL078071, 2018.

Claxton, T., Hossaini, R., Wild, O., Chipperfield, M. P., & Wilson, C.: On the regional and seasonal ozone depletion potential of chlorinated very short-lived substances. Geophys. Res. Lett., 46, 5489– 5498. https://doi.org/10.1029/2018GL081455, 2019.

Chinabaogao. https://free.chinabaogao.com/huagong/201206/062113C592012.html

Claxton, T., Hossaini, R., Wilson, C., Montzka, S. A., Chipperfield, M. P., Wild, O., Bednarz, E. M., Carpenter, L. J., Andrews, S. J., Hackenberg, S. C., Mühle, J., Oram, D., Park, S., Park, M.-K., Atlas, E., Navarro, M., Schauffler, S., Sherry, D., Vollmer, M., Schuck, T., Engel, A., Krummel, P. B., Maione, M., Arduini, J., Saito, T., Yokouchi, Y., O'Doherty, S., Young, D., and 270 Lunder, C.: A synthesis inversion to constrain global emissions of two very short lived chlorocarbons: dichloromethane, and perchloroethylene, J. Geophys. Res.-Atmos., 125, e2019JD031818, https://doi.org/10.1029/2019JD031818, 2020.

Crawford, J. H., Ahn, J.-Y., Al-Saadi, J., Chang, L., Emmons, L. K., Kim, J., Lee, G., Park, J.-H., Park, R. J., Woo, J. H., Song, C.-K., Hong, J.-H., Hong, Y.-D., Lefer, B. L., Lee, M., Lee, T., Kim, S.,

Min, K.-E., Yum, S. S., Shin, H. J., Kim, Y.-W., Choi, J.-S., Park, J.-S., Szykman, J. J., Long, R. W., Jordan, C. E., Simpson, I. J., Fried, A., Dibb, J. E., Cho, S., and Kim, Y. P.: The Korea–United

States Air Quality (KORUS-AQ) field study, Elementa-Sci. Anthrop., 9, 00163, doi.org/10.1525/elementa.2020.00163, 2021.

660   Engel, A., Rigby, M., Burkholder, J. B., Fernandez, R. P., Froidevaux, L., Hall, B. D., et al.: Update on ozone-depleting substances (ODSs) and other gases of interest to the Montreal Protocol. In Scientific assessment of ozone depletion: 2018, Global Ozone Research and Monitoring Project—Report No. 58, Chapter 1. World Meteorological Organization, Geneva, Switzerland, 2018.

ECHA (European Chemicals Agency), 2012. https://echa.europa.eu/documents/10162/c667ff11-b443-3d98-daf9-
665   d6d77727bee1

EPA (Environmental Protection Agency), 2020. https://downloads.regulations.gov/EPA-HQ-OPPT-2018-0427-0030/content.pdf.

Falk, S., Sinnhuber, B.-M., Krysztofiak, G., Jöckel, P., Graf, P., and Lennartz, S. T.: Brominated VSLS and their influence on ozone under a changing climate, Atmos. Chem. Phys., 17, 11313–11329, https://doi.org/10.5194/acp-17-11313-2017,
670   2017.

Falta, R. W, N. Bulsara, J. K. Henderson and R. A. Mayer: Leaded-gasoline additives still contaminate groundwater: Ethylene dibromide and 1,2-dichloroethane persist at high levels despite a phaseout in the late 1980's, but they get little attention, Environ. Sci. Technol., 39, 379A–384A, doi.org/10.1021/es053352k, 2005.

Fang, X., Park, S., Saito, T., Tunnicliffe, R., Ganesan, A. L., Rigby, M., Li, S., Yokouchi, Y., Fraser, P. J., Harth, C. M.,
675   Krummel, P. B., Mühle, J., O'Doherty, S., Salameh, P. K., Simmonds, P. G., Weiss, R. F., Young, D., Lunt, M. F., Manning, 295 A. J., Gressent, A., and Prinn, R. G.: Rapid increase in ozone-depleting chloroform emissions from China, Nat. Geosci., 12, 89–93, 2019.

Feng, W., Chipperfield, M. P., Dorf, M., Pfeilsticker, K., and Ricaud, P.: Mid-latitude ozone changes: studies with a 3-D CTM forced by ERA-40 analyses, Atmos. Chem. Phys., 7, 2357–2369, https://doi.org/10.5194/acp-7-2357-2007, 2007.

680   Feng, W., Chipperfield, M. P., Dhomse, S., Monge-Sanz, B. M., Yang, X., Zhang, K., and Ramonet, M.: Evaluation of cloud convection and tracer transport in a three-dimensional chemical transport model, Atmos. Chem. Phys., 11, 5783–5803, doi:10.5194/acp-11-5783-2011, 2011.

Feng, L., Smith, S. J., Braun, C., Crippa, M., Gidden, M. J., Hoesly, R., Klimont, Z., van Marle, M., van den Berg, M., and van der Werf, G. R.: The generation of gridded emissions data for CMIP6, Geosci. Model Dev., 13, 461–482,
685   doi.org/10.5194/gmd-13-461-2020, 2020.

Fernandez, R. P., Salawitch, R. J., Kinnison, D. E., Lamarque, J.-F., and Saiz-Lopez, A.: Bromine partitioning in the tropical tropopause layer: implications for stratospheric injection, Atmos. Chem. Phys., 14, 13391–13410, doi.org/10.5194/acp-14-13391-2014, 2014.

Fernandez, R. P., Barrera, J. A., López-Noreña, A. I., Kinnison, D. E., Nicely, J., Salawitch, R. J., Wales, P. A., Toselli, B. M., Tilmes, S., Lamarque, J.-F., Cuevas, C. A., and Saiz-Lopez, A.: Intercomparison between surrogate, explicit and full treatments of VSL bromine chemistry within the CAM-Chem chemistry-climate model, Geophys. Res. Lett., 48, e2020GL091125, doi.org/10.1029/2020GL091125, 2021.

Fiehn, A., Quack, B., Hepach, H., Fuhlbrügge, S., Tegtmeier, S., Toohey, M., Atlas, E., and Krüger, K.: Delivery of halogenated very short-lived substances from the west Indian Ocean to the stratosphere during the Asian summer monsoon, Atmos. Chem. Phys., 17, 6723–6741, doi.org/10.5194/acp-17-6723-2017, 2017.

Giannakopoulos, C., Chipperfield, M. P., Law, K. S., and Pyle, J. A.: Validation and intercomparison of wet and dry deposition schemes using 210Pb in a global three-dimensional off-line chemical transport model, J. Geophys. Res., 104, 23761–23784, doi.org/10.1029/1999JD900392, 1999.

Hersbach, H., Bell, B., Berrisford, P., Hirahara, S., Horányi, A., Muñoz-Sabater, J., Nicolas, J., Peubey, C., Radu, R., Schepers, D., Simmons, A., Soci, C., Abdalla, S., Abellan, X., Balsamo, G., Bechtold, P., Biavati, G., Bidlot, J., Bonavita, M., De Chiara, G., Dahlgren, P., Dee, D., Diamantakis, M., Dragani, R., Flemming, J., Forbes, R., Fuentes, M., Geer, A., Haimberger, L., Healy, S., Hogan, R. J., Hólm, E., Janisková, M., Keeley, S., Laloyaux, P., Lopez, P., Lupu, C., Radnoti, G., de Rosnay, P., Rozum, I., Vamborg, F., Villaume, S., and Thépaut, J.-N.: The ERA5 global reanalysis, Q. J. Roy. Meteor. Soc., 146, 1999–315 2049, https://doi.org/10.1002/qj.3803, 2020 (data available at: https://www.ecmwf.int/en/forecasts/datasets/reanalysisdatasets/era5, last access: 12 August 2022).

Hoffmann, L. and Spang, R.: An assessment of tropopause characteristics of the ERA5 and ERA-Interim meteorological reanalyses, Atmos. Chem. Phys., 22, 4019–4046, doi.org/10.5194/acp-22-4019-2022, 2022.

Holtslag, A. and Boville, B.: Local versus nonlocal boundary-layer diffusion in a global climate model, J. Climate, 6, 1825–1842, 1993.

Hossaini, R., Chipperfield, M. P., Montzka, S. A., Leeson, A. A., Dhomse, S., & Pyle, J. A.: The increasing threat to stratospheric ozone from dichloromethane. Nat. Commun., 8, 15962, doi.org/10.1038/ncomms15962, 2017.

Hossaini, R., Atlas, E., Dhomse, S. S., Chipperfield, M. P., Bernath, P. F., Fernando, A. M., Mühle, J., Leeson, A. A., Montzka, S. A., Feng, W., Harrison, J. J., Krummel, P., Vollmer, M. K., Reimann, S., O'Doherty, S., Young, D., Maione, M., Arduini, 320 J., and Lunder, C. R.: Recent trends in stratospheric chlorine from very short-lived substances, J. Geophys. Res.-Atmos., 124, 2318–2335, doi.org/10.1029/2018JD029400, 2019.

Huang, M., Carmichael, G. R., Pierce, R. B., Jo, D. S., Park, R. J., Flemming, J., Emmons, L. K., Bowman, K. W., Henze, D. K., Davila, Y., Sudo, K., Jonson, J. E., Tronstad Lund, M., Janssens-Maenhout, G., Dentener, F. J., Keating, T. J., Oetjen, H., and Payne, V. H.: Impact of intercontinental pollution transport on North American ozone air pollution: an HTAP phase 2 multi-model study, Atmos. Chem. Phys., 17, 5721–5750, doi.org/10.5194/acp-17-5721-2017, 2017.

720 IPCC/TEAP: Safeguarding the Ozone Layer and the Global Climate System: Special Report of the Intergovernmental Panel on Climate Change. Cambridge University Press, 2005.

Jordan A, Stoy P, and Sneddon HF: Chlorinated solvents: their advantages, disadvantages, and alternatives in organic and medicinal chemistry. Chem Rev., 121, 1582–622, doi.org/10.1021/acs.chemrev.0c00709, 2020.

Keber, T., Bönisch, H., Hartick, C., Hauck, M., Lefrancois, F., Obersteiner, F., Ringsdorf, A., Schohl, N., Schuck, T.,
725 Hossaini, R., Graf, P., Jöckel, P., and Engel, A.: Bromine from short-lived source gases in the extratropical northern hemispheric upper troposphere and lower stratosphere (UTLS), Atmos. Chem. Phys., 20, 4105–4132, doi.org/10.5194/acp-20-4105-2020, 2020.

Laube, J. C., Engel, A., Bönisch, H., Möbius, T., Worton, D. R., Sturges, W. T., Grunow, K., and Schmidt, U.: Contribution of very short-lived organic substances to stratospheric chlorine and bromine in the tropics – a case study, Atmos. Chem.
730 Phys., 8, 7325–7334, doi:10.5194/acp-8-7325-2008, 2008.

Laube, J.C., Tegtmeier, S., Fernandez, R.P.F., Harrison, J., Hu, L., Krummel, P., Mahieu, E., Park, S., and Western, L., et al.: .Update on ozone-depleting substances (ODSs) and other gases of interest to the Montreal Protocol. In Scientific assessment of ozone depletion: 2022, GAW Report No. 278, Chapter 1. World Meteorological Organization, Geneva, Switzerland, 2022.

735 Lauther, V., Vogel, B., Wintel, J., Rau, A., Hoor, P., Bense, V., Müller, R., and Volk, C. M.: In situ observations of CH2Cl2 and CHCl3 show efficient transport pathways for very short-lived species into the lower stratosphere via the Asian and the North American summer monsoon, Atmos. Chem. Phys., 22, 2049–2077, doi.org/10.5194/acp-22-2049-2022, 2022.

Li, Q., Jiang, J. H., Wu, D. L., Read, W. G., Livesey, N. J., Waters, J. W., Zhang, Y., Wang, B., Filipiak, M. J., Davis, C. P., Turquety, S., Wu, S., Park, R. J., Yantosca, R. M., and Jacob, D. J.: Convective outflow of South Asian pollution: a global
740 CTM simulation compared with EOS MLS observations, Geophys. Res. Lett., 32, L14826, doi.org/10.1029/2005GL022762, 2005.

Lyu, X., Guo, H., Wang, Y., Zhang, F., Nie, K., Dang, J., Liang, Z., Dong, S., Zeren, Y., Zhou, B., Gao, W., Zhao, S., and Zhang, G.: Hazardous volatile organic compounds in ambient air of China. Chemosphere, 246, 125731, doi.org/10.1016/j.chemosphere.2019.125731, 2020.

745 Monks, S. A., Arnold, S. R., Hollaway, M. J., Pope, R. J., Wilson, C., Feng, W., Emmerson, K. M., Kerridge, B. J., Latter, B. L., Miles, G. M., Siddans, R., and Chipperfield, M. P.: The TOMCAT global chemical transport model v1.6: description of chemical mechanism and model evaluation, Geosci. Model Dev., 10, 3025–3057, doi.org/10.5194/gmd-10-3025-2017, 2017.

Müller, S., Hoor, P., Bozem, H., Gute, E., Vogel, B., Zahn, A., Bönisch, H., Keber, T., Krämer, M., Rolf, C., Riese, M.,
750 Schlager, H., and Engel, A.: Impact of the Asian monsoon on the extratropical lower stratosphere: trace gas observations during TACTS over Europe 2012, Atmos. Chem. Phys., 16, 10573–10589, doi.org/10.5194/acp-16-10573-2016, 2016.

Oram, D. E., Ashfold, M. J., Laube, J. C., Gooch, L. J., Humphrey, S., Sturges, W. T., Leedham Elvidge, E. C., Forster, G. L., Harris, N. R. P., Mead, M. I., Samah, A. A., Phang, S. M., Ou-Yang, C.-F., Lin, N.-H., Wang, J.-L., Baker, A. K., Brenninkmeijer, C. A. M., and Sherry, D.: A growing threat to the ozone layer from short-lived anthropogenic
755 chlorocarbons, Atmos. Chem. Phys., 17, 11929–11941, doi.org/10.5194/acp-17-11929-2017, 2017.

Pan, L.L., Atlas, E.L., Honomichl, S.B., Newman, P.A., et al.: East Asian summer monsoon delivers large abundances of very short-lived organic chlorine substances to the lower stratosphere, PNAS, 121, e2318716121, doi.org/10.1073/pnas.2318716121, 2024.

Patra, P. K., Houweling, S., Krol, M., Bousquet, P., Belikov, D., Bergmann, D., Bian, H., Cameron-Smith, P., Chipperfield,
760 M. P., Corbin, K., Fortems-Cheiney, A., Fraser, A., Gloor, E., Hess, P., Ito, A., Kawa, S. R., Law, R. M., Loh, Z., Maksyutov, S., Meng, L., Palmer, P. I., Prinn, R. G., Rigby, M., Saito, R., and Wilson, C.: TransCom model simulations of CH4 and related species: linking transport, surface flux and chemical loss with CH4 variability in the troposphere and lower stratosphere, Atmos. Chem. Phys., 11, 12813–12837, doi.org/10.5194/acp-11-12813-2011, 2011.

Perrette, M.: ISI-MIP/isipedia-countries (v2.6). GitHub repository. https://github.com/ISI-MIP/isipedia-
765 countries/releases/tag/v2.6, 2013.

Prather, M.: Numerical advection by conservation of second-order moments, J. Geophys. Res., 91, 6671–6681, 1986.

Randel, W. J. and Park, M.: Deep convective influence on the Asian summer monsoon anticyclone and associated tracer variability observed with Atmospheric Infrared Sounder (AIRS), J. Geophys. Res., 111, D12314, doi.org/10.1029/2005JD006490, 2006.

770 Randel, W. J., Park, M., Emmons, L., Kinnison, D., Bernath, P., Walker, K. A., Boone, C., and Pumphrey, H.: Asian monsoon transport of pollution to the stratosphere, Science, 328, 611–613,

doi:10.1126/science.1182274, 2010.

Roozitalab, B., Emmons, L. K., Hornbrook, R. S., Kinnison, D. E., Fernandez, R. P., Li, Q., et al.: Measurements and modeling of the interhemispheric differences of atmospheric chlorinated very

775 short-lived substances. J. Geophys. Res.-Atmos., 129, e2023JD039518, doi.org/10.1029/2023JD03951, 2014.

Saiz-Lopez, A., Baidar, S., Cuevas, C. A., Koenig, T., Fernandez, R. P., Dix, B., Kinnison, D. E., Lamarque, J.-F., Rodriguez-Lloveras, X., and Campos, T. L.: Injection of iodine to the stratosphere, Geophys. Res. Lett., 42, 6852–6859, doi.org/10.1002/2015GL064796, 2015.

Salawitch, R., Weisenstein, D., Kovalenko, L., Sioris, C., Wennberg, P., Chance, K., Ko, M., and McLinden, C.: Sensitivity of ozone to bromine in the lower stratosphere, Geophys. Res. Lett., 32, L05811, doi:10.1029/2004GL021504, 2005.

Sander, R.: Compilation of Henry's law constants (version 5.0.0) for water as solvent, Atmos. Chem. Phys., 23, 10901–12440, https://doi.org/10.5194/acp-23-10901-2023, 2023.

Say, D., Ganesan, A. L., Lunt, M. F., Rigby, M., O'Doherty, S., Harth, C., Manning, A. J., Krummel, P. B., and Bauguitte, S.: Emissions of halocarbons from India inferred through atmospheric measurements, Atmos. Chem. Phys., 19, 9865–9885, doi.org/10.5194/acp-19-9865-2019, 2019.

Sherwood, J.: European restrictions on 1,2-dichloroethane: C-H activation research and development should be liberated and not limited. Angew. Chem. Int. Ed. 57, 14286–14290, doi.org/10.1002/anie.201800549 2018.

Singh, H. B., Brune, W. H., Crawford, J. H., Flocke, F., and Jacob, D. J.: Chemistry and transport of pollution over the Gulf of Mexico and the Pacific: spring 2006 INTEX-B campaign overview and first results, Atmos. Chem. Phys., 9, 2301–2318, doi.org/10.5194/acp-9-2301-2009, 2009.

Simpson, I. J., Blake, D. R., Blake, N. J., Meinardi, S., Barletta, B., Hughes, S. C., Fleming, L. T., Crawford, J. H., Diskin, G. S., Emmons, L. K., Fried, A., Guo, H., Peterson, D. A., Wisthaler, A., Woo, J.-H., Barré, J., Gaubert, B., Kim, J., Kim, M. J., Kim, Y., Knote, C., Mikoviny, T., Pusede, S. E., Schroeder, J. R., Wang, Y., Wennberg, P. O., and Zeng, L.: Characterization, sources and reactivity of volatile organic compounds (VOCs) in Seoul and surrounding regions during KORUS-AQ, Elem. Sci. Anth., 8, 37, doi.org/10.1525/elementa.434, 2020.

TEAP (Technology and Economic Assessment Panel): UNEP 2022 Report Of The Medical And Chemical Technical Options Committee (MCTOC), 2022.

Tiedtke, M.: A comprehensive mass flux scheme for cumulus parameterization in large-scale models, Mon. Weather Rev., 117, 1779–1800, doi:10.1175/1520- 0493(1989)1172.0.CO;2, 1989.

UNEP (United National Environment Programme): 2002. https://hpvchemicals.oecd.org/ui/handler.axd?id=95f8d194-732a-4cc9-b59b-839ed3b18732

Villamayor, J., Iglesias-Suarez, F., Cuevas, C.A. et al.: Very short-lived halogens amplify ozone depletion trends in the tropical lower stratosphere, Nat. Clim. Chang., 13, 554–560, doi.org/10.1038/s41558-023-01671-y, 2023.

Von Hobe, M., Grooß, J.-U., Günther, G., Konopka, P., Gensch, I., Krämer, M., Spelten, N., Afchine, A., Schiller, C., Ulanovsky, A., Sitnikov, N., Shur, G., Yushkov, V., Ravegnani, F., Cairo, F., Roiger, A., Voigt, C., Schlager, H., Weigel, R., Frey, W., Borrmann, S., Müller, R., and Stroh, F.: Evidence for heterogeneous chlorine activation in the tropical UTLS, Atmos. Chem. Phys., 11, 241–256, doi.org/10.5194/acp-11-241-2011, 2011.

Wang, C., Shao, M., Huang, D., Lu, S., Zeng, L., Hu, M., and Zhang, Q.: Estimating halocarbon emissions using measured ratio relative to tracers in China, Atmos. Environ., 89, 816–826, doi.org/10.1016/j.atmosenv.2014.03.025, 2014.

810 WMO (World Meteorological Organization): Scientific Assessment of Ozone Depletion: 2018, Global Ozone Research and Monitoring Project-Report No. 58, WMO, Geneva, Switzerland, 2018.

WMO (World Meteorological Organization): Scientific Assessment of Ozone Depletion: 2022, Global Ozone Research and Monitoring Project. GAW Report No. 278, WMO, Geneva, Switzerland, 2022.

Wofsy, S. C., Team, H. S., Team, C. M., and Team, S.: HIAPER Pole-to-Pole Observations (HIPPO): fine-grained,
815 globalscale measurements of climatically important atmospheric gases and aerosols, Philos. T. R. Soc., 369, 2073–2086, doi:10.1098/rsta.2010.0313, 2011.

Zou, H., Wang, T., Wang, Z.L. et al: Continuing large-scale global trade and illegal trade of highly hazardous chemicals. Nat Sustain., doi.org/10.1038/s41893-023-01158-w, 2023.